BIOCHEMISTRY
including biophysical chemistry & molecular biology

Article

pubs.acs.org/biochemistry

Evidence from FTIR Difference Spectroscopy That D1-Asp61 Influences the Water Reactions of the Oxygen-Evolving Mn_4CaO_5 Cluster of Photosystem II

Richard J. Debus*

Department of Biochemistry, University of California, Riverside, California 92521, United States

ABSTRACT: Understanding the mechanism of photosynthetic water oxidation requires characterizing the reactions of the water molecules that serve as substrate or that otherwise interact with the oxygen-evolving Mn_4CaO_5 cluster. FTIR difference spectroscopy is a powerful tool for studying the structural changes of hydrogen bonded water molecules. For example, the O−H stretching mode of water molecules having relatively weak hydrogen bonds can be monitored near 3600 cm^{-1}, the D-O-D bending mode can be monitored near 1210 cm^{-1}, and highly polarizable networks of hydrogen bonds can be monitored as broad features between 3000 and 2000 cm^{-1}. The two former regions are practically devoid of overlapping vibrational modes from the protein. In Photosystem II, water oxidation requires a precisely choreographed sequence of proton and electron transfer steps in which proton release is required to prevent the redox potential of the Mn_4CaO_5 cluster from rising to levels that would prevent its subsequent oxidation. Proton release takes place via one or more proton egress pathways leading from the Mn_4CaO_5 cluster to the thylakoid lumen. There is growing evidence that D1-D61 is the initial residue of one dominant proton egress pathway. This residue interacts directly with water molecules in the first and second coordination spheres of the Mn_4CaO_5 cluster. In this study, we explore the influence of D1-D61 on the water reactions accompanying oxygen production by characterizing the FTIR properties of the D1-D61A mutant of the cyanobacterium, *Synechocystis* sp. PCC 6803. On the basis of mutation-induced changes to the carbonyl stretching region near 1747 cm^{-1}, we conclude that D1-D61 participates in the same extensive networks of hydrogen bonds that have been identified previously by FTIR studies. On the basis of mutation-induced changes to the weakly hydrogen-bonded O−H stretching region, we conclude that D1-D61 interacts with water molecules that are located near the $Cl^-(1)$ ion and that deprotonate or participate in stronger hydrogen bonds as a result of the S_1 to S_2 and S_2 to S_3 transitions. On the basis of the elimination of a broad feature between 3100 and 2600 cm^{-1}, we conclude that the highly polarizable network of hydrogen bonds whose polarizability or protonation state increases during the S_1 to S_2 transition involves D1-D61. On the basis of the elimination of features in the D-O-D bending region, we conclude that D1-D61 forms a hydrogen bond to one of the H_2O molecules whose H−O−H bending mode changes in response to the S_1 to S_2 transition. The elimination of this H_2O molecule in the D1-D61A mutant provides one rationale for the decreased efficiency of water oxidation in this mutant. Finally, we discuss reasons why the recent conclusion that a substrate-containing cluster of five water molecules accepts a proton from the Mn_4CaO_5 cluster during the S_1 to S_2 transition and deprotonates during subsequent S state transitions should be reassessed.

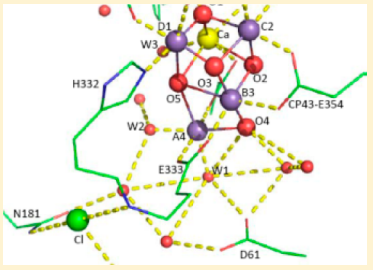

The light-driven oxidation of water in photosystem II (PSII) produces nearly all of the O_2 on Earth and drives the production of nearly all of its biomass. Photosystem II is an integral membrane protein complex that is located in the thylakoid membranes of plants, algae, and cyanobacteria.[1−4] It is a homodimer *in vivo*, having a total molecular weight of approximately 700 kDa with each monomer containing at least 20 different subunits and nearly 60 organic and inorganic cofactors including 35 Chl *a*, 11 carotenoid, 2 pheophytin, and 2 plastoquinone molecules. The O_2-evolving catalytic center in PSII consists of a Mn_4CaO_5 cluster and its immediate protein environment. In response to photochemical events within PSII, the Mn_4CaO_5 cluster accumulates four oxidizing equivalents and then catalyzes the oxidation of two molecules of water, releasing one molecule of O_2 as a byproduct.[5−10] The Mn_4CaO_5 cluster serves as the interface between single-electron photochemistry and the four-electron process of water oxidation. The photochemical events that precede water oxidation take place in a heterodimer of two 38−39 kDa polypeptides known as D1 and D2. These events are initiated by the transfer of excitation energy to the photochemically active Chl *a* multimer known as P_{680} following the capture of light energy by the antenna complex. Excitation of P_{680} results in the formation of the charge-separated state, $P_{680}^{\bullet+}Pheo^{\bullet-}$. This light-induced separation of charge is stabilized by the rapid oxidation of $Pheo^{\bullet-}$ by Q_A, the primary plastoquinone electron acceptor, and by the rapid reduction of $P_{680}^{\bullet+}$ by Y_Z, one of two redox-active tyrosine residues in PSII. The resulting $Y_Z^{\bullet}$ radical in turn oxidizes the Mn_4CaO_5 cluster, while $Q_A^{\bullet-}$ reduces the secondary plastoquinone, Q_B. Subsequent charge separations

Received: March 12, 2014
Revised: April 12, 2014
Published: April 14, 2014

result in further oxidation of the Mn_4CaO_5 cluster and in the two-electron reduction and protonation of Q_B to form plastoquinol, which subsequently exchanges into the membrane-bound plastoquinone pool. During each catalytic cycle, the Mn_4CaO_5 cluster advances through five oxidation states termed S_n, where "n" denotes the number of oxidizing equivalents that are stored (n = 0−4). The S_1 state predominates in dark-adapted samples. The S_4 state is a transient intermediate whose formation triggers the formation and release of O_2 and the regeneration of the S_0 state.

In the recent 1.9 Å crystallographic structural model of PSII (PDB: 3ARC),[11,12] and in subsequent computational refinements of the structure of the Mn_4CaO_5 cluster and its ligation environment,[13−18] the cluster is arranged as a distorted Mn_3CaO_4 cube that is linked to a fourth "dangling" Mn ion (denoted Mn_{A4} (we have adopted the combined crystal structure and EPR-based notation for the Mn ions advanced in refs 8 and 9)) by one corner oxo bridge (denoted O5) and by an additional oxygen bridging ligand (see Figure 1). The cluster's Mn and Ca ions are ligated by six carboxylate groups and one histidine residue, all but one of which are supplied by the D1 polypeptide. Numerous immobilized water molecules are located on or near the Mn_4CaO_5 cluster, including two that are bound to Mn_{A4} (these are denoted W1 and W2) and two that are bound to the Ca ion (these are denoted W3 and W4). In recent proposals for the mechanism of O−O bond formation, O5 derives from one of the two substrate water molecules and becomes incorporated into the product dioxygen molecule by reacting with another substrate-water-derived Mn or Ca ligand.[8,9,19−25] Recent pulsed EPR studies conducted in combination with measurements of water exchange rates have provided support for these proposals by providing strong evidence that O5 corresponds to the slowly exchanging substrate water molecule.[22,25] The rapidly exchanging substrate water molecule is considered to be W2, W3, or a water molecule that binds to Mn_{D1} during the S_2 to S_3 transition [possibly moving from a site on Mn_{A4}[25]]. Structural flexibility of the Mn_4CaO_5 cluster is a key aspect of these proposals, and there is an emerging consensus that the Mn_4CaO_5 cluster readily interconverts between two nearly isoenergetic conformers during the S state cycle, with O5 ligating the dangling Mn_{A4} ion in one conformer (giving rise to the multiline EPR signal in the S_2 state) and ligating Mn_{D1} in the other (giving rise to the g = 4.1 EPR signal in the S_2 state)[8,9,18,26−28] [also see ref 16]. In the S_2 state, this interconversion is linked to a redox isomerization, with the Mn ion *not* binding O5 being in its Mn(III) oxidation state in addition to having an open coordination position along its Jahn−Teller axis. A similar structural conversion involving changes in the ligation of O5 during the S_2 to S_3 transition has also been proposed on the basis of a recent Mn-EXAFS study.[29]

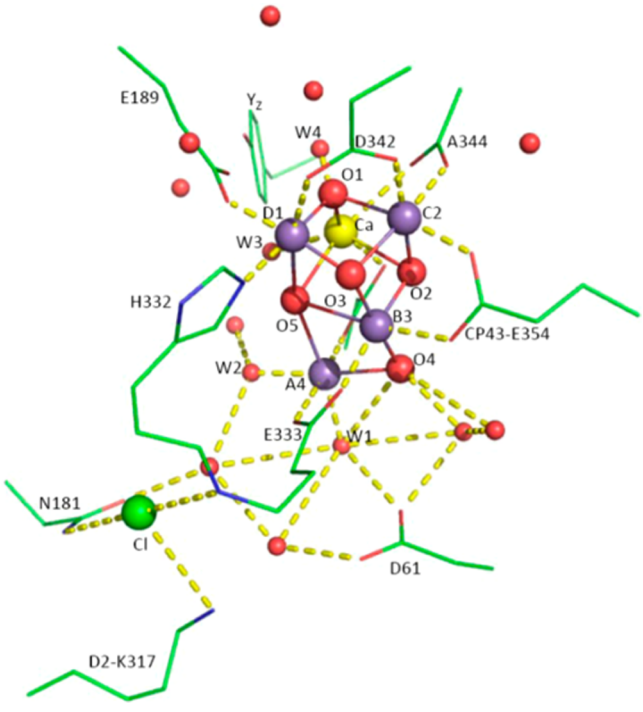

Figure 1. Mn_4CaO_5 cluster and its environment[11] showing the position of D1-Asp61 in relation to nearby water molecules. For clarity, only selected residues are shown. Except as noted otherwise, all residues are from the D1 polypeptide. Purple spheres, manganese ions [the labels A4, B3, C2, and D1 reflect the combined crystal structure and EPR-based notations for the Mn ions advanced in refs 8 and 9]; yellow sphere, calcium; large red spheres, μ-oxo bridges; green sphere, chloride; small red spheres, water molecules including the four water molecules bound to Mn_{A4} (W1 and W2) and Ca (W3 and W4).

Water oxidation in PSII involves a precisely choreographed sequence of proton and electron transfer steps in which the release of protons is required to prevent the redox potential of the Mn_4CaO_5 cluster from rising to levels that would prevent its subsequent oxidation by $Y_Z^{\bullet}$.[30−34] This choreography is characterized by a strictly alternating removal of electrons and protons from the Mn_4CaO_5 cluster during the S state cycle, with proton transfer preceding the oxidation of the Mn_4CaO_5 cluster during the S_2 to S_3 and S_3 to S_4 transitions.[7,21,31,32,34,35] During the S_2 to S_3 and S_3 to S_4 transitions, the trigger for proton transfer is proposed to be the formation of $Y_Z^{\bullet}$, with the positive charge on the $Y_Z^{\bullet}$/D1-His190 pair inducing the deprotonation of CP43-Arg357[30,33,36,37] or a nearby cluster of water molecules.[35] In these proposals, the subsequent oxidation of the Mn_4CaO_5 cluster involves the simultaneous transfer of a proton from the Mn_4CaO_5 cluster to the now deprotonated CP43-Arg357 or water cluster. The deprotonation of CP43-Arg357 (or the cluster of water molecules) is envisioned to take place via one or more proton egress pathways or "channels" leading from the Mn_4CaO_5 cluster to the thylakoid lumen. The "channels" are expected to be composed of networks of hydrogen bonds involving protonatable amino acid side chains and water molecules. Several possible channels for water access, O_2 egress, and proton egress have been identified in the 1.9 Å[11,12] and earlier 3.5 Å to 2.9 Å[38−40] crystallographic structural models on the basis of visual examinations,[11,38,41−44] electrostatic calculations,[45] solvent accessibility simulations,[46] cavity searching algorithms,[40,47,48] molecular dynamics simulations of water diffusion,[49−52] and the identification of oxidatively modified amino acid residues in the interior of PSII[53,54] [for reviews, see refs 44 and 55−57].

In most postulated proton egress pathways, D1-D61 is the closest residue to the Mn_4CaO_5 cluster.[44,55−57] Characterizations of D1-D61A and D1-D61N thylakoid membranes and PSII core complexes have provided evidence that D1-D61 is the initial residue of a dominant proton egress pathway leading to the lumen.[58−61] In the 1.9 Å structural model,[11,12] this residue shares W1 with the dangling Mn_{A4} ion, shares another water molecule with oxo bridge O4, and interacts indirectly (via two water molecules) with W2. Consequently, D1-D61 interacts

dx.doi.org/10.1021/bi500309f | *Biochemistry* 2014, 53, 2941−2955

directly with water molecules in the first and second coordination spheres of the Mn and Ca ions of the Mn_4CaO_5 cluster. Mutation of this residue would likely alter the response of several water molecules to the oxidations of the cluster that accompany the S state transitions.

FTIR difference spectroscopy is an extremely sensitive tool for characterizing dynamic structural changes that occur during an enzyme's catalytic cycle.[62−66] In PSII, the frequencies of numerous vibrational modes change as the Mn_4CaO_5 cluster is oxidized through the S state cycle, including many modes that are attributable to carboxylate residues and hydrogen-bonded water molecules.[67−70] FTIR difference spectroscopy has been applied to the study of the structural changes of hydrogen-bonded water molecules in a number of systems including bacteriorhodopsin,[71−76] other Type-1 rhodopsins,[77] bacterial reaction centers,[78−80] cytochrome *c* oxidase,[81] and PSII.[82−85] For example, the O−H stretching mode of water molecules having relatively weak hydrogen bonds can be monitored between 3700 and 3500 cm^{-1},[71,72,75−77,80−88] a region that is devoid of overlapping vibrational modes from the protein. Another example is the H−O−H bending mode. This mode appears near 1640 cm^{-1}, is sensitive to hydrogen bonding, and disappears when the H_2O molecule is deprotonated.[85] Unfortunately, these modes are weak, and the 1640 cm^{-1} region overlaps the strong absorption bands of the amide I groups of the polypeptide backbone. However, the D-O-D bending mode can be monitored near 1210 cm^{-1}, a region that is practically devoid of other protein vibrational modes.[85] Finally, highly polarizable networks of hydrogen bonds can be monitored as broad features between 3000 and 2000 cm^{-1}.[74,75,78−80,83] In a series of landmark studies, Noguchi and co-workers have provided evidence for (i) a change in the hydrogen-bond strength of a water molecule having a highly asymmetric hydrogen-bond structure during the S_1 to S_2 transition,[82] (ii) deprotonations or changes in hydrogen-bond strengths of water molecules during the other S state transitions,[83] (iii) increases in the polarizability or protonation state of highly polarizable network(s) of hydrogen bonds during each S state transition,[83,89] and (iv) changes in the structure of a least two fully protonated water molecules during each S state transition.[85] The latter study also provided evidence that substrate water inserts into the Mn_4CaO_5 cluster from a bound water cluster during the S_2 to S_3 and S_3 to S_0 transitions,[85] although these water molecules may bind to "holding" sites and become the substrate on the next turnover. In the current study, we apply these methods to explore the influence of D1-D61 on the water reactions of the Mn_4CaO_5 cluster. We also discuss the recent conclusion[90] that a substrate-containing cluster of five water molecules accepts a proton during the S_1 to S_2 transition and deprotonates during subsequent S state transitions.

MATERIALS AND METHODS

Construction of Mutants and Propagation of Cultures. Construction of the D1-D61A mutation was described previously: the mutation was introduced into the *psbA-2* gene of *Synechocystis* sp. PCC 6803[91] and transformed into a host strain of *Synechocystis* that lacks all three *psbA* genes and contains a hexahistidine-tag (His-tag) fused to the C-terminus of CP47.[92] Single colonies were selected for the ability to grow on solid media containing 5 μg/mL kanamycin monosulfate. Solid media contained 5 mM glucose and 10 μM DCMU. The DCMU and antibiotic were omitted from the liquid cultures. Large-scale liquid cultures (each consisting of three 7-L cultures held in glass carboys) were propagated as described previously.[93] To verify the integrity of the mutant cultures that were harvested for the purification of PSII core complexes, an aliquot of each culture was set aside, and the sequence of the relevant portion of the *psbA-2* gene was obtained after PCR amplification of genomic DNA.[91] No traces of the wild-type codon was detected in any of the mutant cultures.

Purification of Thylakoid Membranes. Thylakoid membranes were isolated under dim green light at 4 °C with a procedure[94] modified from that of Tang and Diner.[95] Harvested cells were concentrated and suspended in a buffer containing 1.2 M betaine, 10% (v/v) glycerol, 50 mM MES-NaOH (pH 6.0), 5 mM $CaCl_2$, 5 mM $MgCl_2$, 1 mM benzamidine, 1 mM ε-amino-*n*-caproic acid, 1 mM phenymethylsulfonyl fluoride, and 0.05 mg/mL DNase I, then broken by nine cycles of (5 s on/15 min off) in a glass bead homogenizer (Bead-Beater, BioSpec Products, Bartlesville, OK). (The use of betaine was suggested to us by ref 96.) After the separation of unbroken cells and debris by low speed centrifugation, the resulting thylakoid membranes were concentrated by ultracentrifugation (20 min at 40,000 rpm in a Beckman Ti45 rotor) and suspended to a concentration of 1.0−1.5 mg of Chl/mL in TM buffer [1.2 M betaine, 10% (v/v) glycerol, 50 mM MES-NaOH (pH 6.0), 20 mM $CaCl_2$, and 5 mM $MgCl_2$]. The concentrated thylakoid membranes were used immediately for the purification of PSII core complexes.

Purification of PSII Core Complexes. Oxygen-evolving PSII core complexes were purified under dim green light at 4 °C as described previously.[94] To a suspension of freshly prepared thylakoid membranes (60−100 mg of Chl), the detergent *n*-dodecyl β-D-maltoside (Anatrace Inc., Maumee, OH) was added dropwise with gentle stirring from a stock of 10% (w/v) detergent (dissolved in TM buffer) to final concentrations of 1 mg of Chl/mL and 1% (w/v) detergent.[95] Extraction was allowed to proceed with gentle stirring for an additional 10 min in darkness. Unsolubilized material was pelleted by centrifuging at 17,500 rpm in a Beckman JA-20 rotor for 10 min.[97] The supernatant was loaded at a flow rate of 2.5 mL/min onto 40 mL of Ni-NTA superflow affinity resin (Qiagen, Inc., Valencia, CA) that had been packed in a 5 cm diameter chromatography column and equilibrated with PSII buffer [1.2 M betaine, 10% (v/v) glycerol, 50 mM MES-NaOH (pH 6.0), 20 mM $CaCl_2$, 5 mM $MgCl_2$, and 0.03% (w/v) *n*-dodecyl β-D-maltoside]. After loading, the column was washed at a flow rate of 5 mL/min with four bed volumes of PSII buffer and then eluted at the same flow rate with four bed volumes of PSII buffer containing 50 mM histidine. The eluent was brought to 1 mM EDTA and concentrated by ultrafiltration [Amicon Models 2000 and 8400 stirred cells fitted with YM-100 membranes, followed by Amicon Ultra-4 100 K centrifugal filter devices (EMD Millipore, Billerica, MA)] to approximately 1 mg of Chl/mL. The purified PSII core complexes [in 1.2 M betaine, 10% (v/v) glycerol, 50 mM MES-NaOH (pH 6.0), 20 mM $CaCl_2$, 5 mM $MgCl_2$, 50 mM histidine, 1 mM EDTA, and 0.03% (w/v) *n*-dodecyl β-D-maltoside] were aliquotted, frozen in liquid N_2, and stored at −196 °C (vapor phase nitrogen).

Preparation of FTIR Samples. All manipulations were conducted under dim green light at 4 °C. Samples (50 μg of Chl *a*) were exchanged into FTIR analysis buffer [40 mM sucrose, 10 mM MES-NaOH (pH 6.0), 5 mM $CaCl_2$, 5 mM NaCl, and 0.06% (w/v) *n*-dodecyl β-D-maltoside[98,99]] by passage through a centrifugal gel filtration column at 27*g*.[100]

dx.doi.org/10.1021/bi500309f | *Biochemistry* 2014, 53, 2941−2955

They were then concentrated to 3.3 mg of Chl/mL with Amicon Ultra-0.5 mL 100 K centrifugal filter devices (EMD Millipore, Billerica, MA). Concentrated samples (6 μL in volume) were mixed with 1/10 volume of fresh 100 mM potassium ferricyanide (dissolved in water), spread to a diameter of about 13 mm in the center of a 25 × 2 mm diameter BaF_2 window, then dried lightly (until tacky) under a stream of dry nitrogen gas. To maintain the sample at 99% relative humidity in the FTIR sample compartment, four 1 μL drops of a solution of 20% (v/v) glycerol in water were spotted around the periphery of the window, not touching the sample.[101] A second BaF_2 window was placed over the first, with a 23 × 1 mm nitrile O-ring acting as a spacer. The sample assembly was sealed into an aluminum cell, loaded into a water-jacketed aluminum holder in the FTIR sample compartment, allowed to equilibrate in darkness for 1.5 h, given 6 pre-flashes, and allowed to dark adapt for 30 min. The sample was kept at a constant temperature of 0 °C by circulating a cold solution of 50% (v/v) ethylene glycol in water through the sample cell holder. Sample concentrations were adjusted so that the absolute absorbance of the amide I band at 1657 cm^{-1} was 0.6−1.1. For the preparation of samples having natural abundance $H_2{}^{16}O$ exchanged for $H_2{}^{18}O$, lightly dried samples were rehydrated with four 1 μL drops of a solution of 20% (v/v) glycerol in $H_2{}^{18}O$ (97% ^{18}O, Cambridge Isotope Laboratories, Inc., Andover, MA). For the preparation of samples having natural abundance $H_2{}^{16}O$ exchanged for $D_2{}^{16}O$ or $D_2{}^{18}O$, lightly dried samples were rehydrated with four 1 μL drops of a solution of 20% (v/v) glycerol$(OD)_3$ (98% D, Cambridge Isotope Laboratories, Inc., Andover, MA) in $D_2{}^{16}O$ (99.9% D, Cambridge Isotope Laboratories, Inc., Andover, MA) or $D_2{}^{18}O$ (98% D, 97% 18O, Cambridge Isotope Laboratories, Inc., Andover, MA), respectively.[85]

FTIR Spectra. Midfrequency FTIR spectra were recorded with a Bruker Vertex 70 spectrometer (Bruker Optics, Billerica, MA) that was equipped with a KBr beam splitter and a preamplified, midrange D317 photovoltaic MCT detector (Kolmar Technologies, Inc., Newburyport, MA). Long-pass 2.4 μm cutoff filters (Andover Corp., Salem, NH) were mounted on both sides of the sample compartment to prevent the interferometer's coaxial helium−neon laser from illuminating the sample and to protect the MCT detector from scattered actinic illumination. Double-sided forward−backward interferograms were recorded with a scanner velocity of 120 kHz. For the calculation of Fourier transforms, a Blackman-Harris 3-term apodization function and a zero-fill factor of 2 were employed. The spectral resolution for all spectra was 4 cm^{-1}. Actinic illumination consisted of flashes (~20 mJ/flash, ~7 ns fwhm) provided by a frequency-doubled Q-switched Nd:YAG laser (BRIO (Quantel USA, Bozeman, MT)). Flash excitation was controlled from the Vertex 70 OPUS interface. The Nd:YAG laser was programmed to deliver a single Q-switched flash during a 20 Hz flashlamp repetition series to ensure the uniformity of the laser light intensity. For each sample, after dark adaptation, six successive flashes were applied with an interval of 13 s between each (no preflashes were applied). Two single-beam spectra were recorded before the first flash, and one single-beam spectrum was recorded starting 0.33 s after the first and subsequent flashes (each single-beam spectrum consisted of 100 scans). The 0.33 s delay was incorporated to allow for the oxidation of $Q_A{}^{\bullet-}$ by the ferricyanide. To obtain difference spectra corresponding to successive S-state transitions, the single-beam spectrum that was recorded after the *n*th flash was divided by the single-beam spectrum that was recorded immediately before the *n*th flash, and the ratio was converted to units of absorption. To estimate the background noise level, the second preflash single-beam spectrum was divided by the first, and the ratio was converted to units of absorption. The sample was dark-adapted for 30 min, then the cycle was repeated. The cycle was repeated 15 times for each sample, and the difference spectra recorded with numerous samples were averaged.

Other Procedures. Chlorophyll concentrations were determined as described previously.[102]

RESULTS

Midfrequency Region. The midfrequency FTIR difference spectra induced by four successive flashes given to the wild-type and D1-D61A PSII core complexes from *Synechocystis* sp. PCC 6803 are compared in Figure 2 (black and red traces, respectively). The spectra that are induced by the first, second, third, and fourth flashes applied to the wild-type PSII core complexes correspond predominantly to the S_2-*minus*-S_1, S_3-

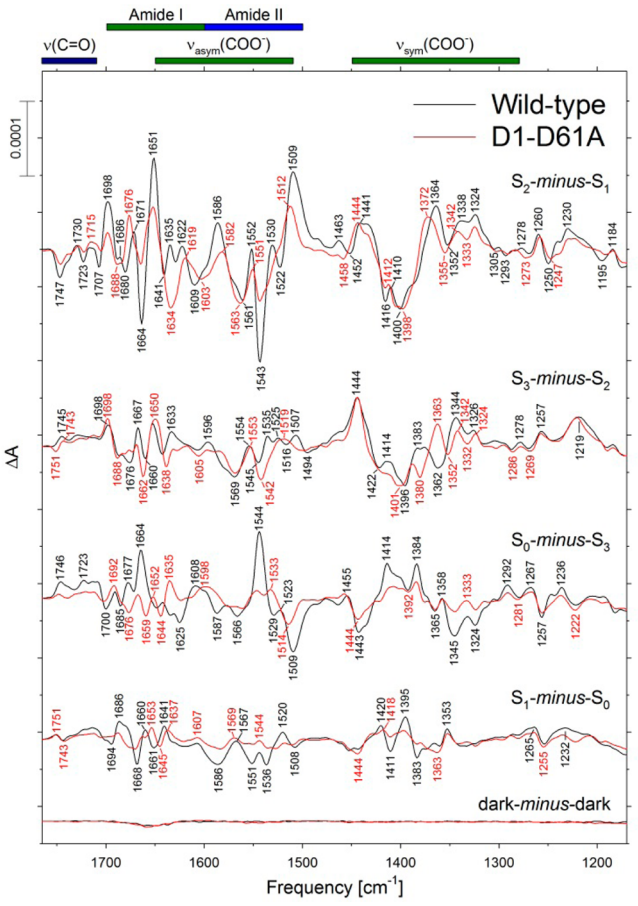

Figure 2. Comparison of the midfrequency FTIR difference spectra of wild-type (black) and D1-D61A (red) PSII core complexes in response to four successive flash illuminations applied at 0 °C. The data (plotted from 1770 to 1170 cm^{-1}) represent the averages of 16 wild-type and 16 D1-D61A samples (24,000 scans for each trace). To facilitate comparisons, the mutant spectra have been multiplied vertically by factors of 1.13, 1.01, 1.0, and 1.0, respectively, after normalization to the average absolute amplitudes of the samples at the amide I peak at 1657 cm^{-1}. Dark-*minus*-dark control traces are included to show the noise level (lower traces).

dx.doi.org/10.1021/bi500309f | *Biochemistry* 2014, 53, 2941−2955

minus-S_2, S_0-*minus*-S_3, and S_1-*minus*-S_0 FTIR difference spectra, respectively.[67−70] The spectra for D1-D61A resemble the spectra we reported previously for this mutant[60] but with an improved signal-to-noise ratio. As shown previously, the S_2-*minus*-S_1 FTIR difference spectrum of D1-D61A PSII core complexes (upper red trace in Figure 2) shows substantial differences from the wild-type spectrum in the amide I and overlapping amide II/$\nu_{asym}(COO^-)$ regions, with positive peaks at 1635 and 1622 cm^{-1} being replaced by a derivative-shaped feature at 1634(−)/1619(+) cm^{-1}, the positive feature at 1586 cm^{-1} being downshifted to 1582 cm^{-1} and being sharply decreased in amplitude, peaks at 1552(+) and 1543(−) cm^{-1} being sharply decreased in amplitude, the positive feature at 1509 cm^{-1} being upshifted to 1512 cm^{-1} and sharply decreased in amplitude, and the 1530(+)/1522(−) cm^{-1} feature being eliminated. The 1635 and 1622 cm^{-1} bands have been identified as amide I modes because both downshift significantly after global incorporation of ^{13}C[98,103] but not appreciably after global incorporation of ^{15}N.[98,103] The 1552(+), 1543(−), 1530(+), and 1522(−) cm^{-1} bands have been identified as amide II modes because all four bands downshift appreciably after global incorporation of ^{13}C[98,103−105] or ^{15}N.[98,103,105−107] The 1587 cm^{-1} band has been assigned to a $\nu_{asym}(COO^-)$ mode because it downshifts by 30−35 cm^{-1} after global incorporation of ^{13}C[98,103−105] but is largely insensitive to the global incorporation of ^{15}N.[98,103,105−107] The 1509 cm^{-1} band appears to consist of overlapping amide II and $\nu_{asym}(COO^-)$ modes.[98,103,105−107] The numerous mutation-induced changes in the amide I and amide II regions show that the mutation substantially alters the response of the protein backbone to the positive charge that develops on the Mn_4CaO_5 cluster during the S_1 to S_2 transition. In contrast to our previous report,[60] the amplitude of the negative peak at 1747 cm^{-1} in the carbonyl stretching [ν(C=O)] region of the spectrum was decreased in amplitude by the mutation (see the expanded version of this region in Figure 3, upper left trace).

In contrast to our previous study,[60] the FTIR difference spectrum that was produced by the second flash applied to D1-D61A PSII core complexes appears to correspond primarily to the S_2 to S_3 transition (the difference between the two studies may be the result of inaccurate sample temperature readings in the earlier study): only the negative features at 1638 and 1542 cm^{-1} resemble features in the S_2-*minus*-S_1 FTIR difference spectrum of this mutant (compare the upper two red traces in Figure 2). The primary differences between the S_3-*minus*-S_2 spectra of the wild type and D1-D61A, besides the appearance of the 1638(−) and 1542(−) features just mentioned, appear to be in the symmetric carboxylate stretching [$\nu_{sym}(COO^-)$] region, with a 1383(+)/1362(−) feature in the wild type being replaced with a 1380(−)/1363(+) feature in the mutant. As in our previous report,[60] the positive peak at 1745 cm^{-1} in the ν(C=O) region was replaced by a 1751(−)/1743(+) feature (see Figure 3, lower left trace).

The FTIR difference spectra that were produced by the third and fourth flashes applied to the D1-D61A PSII core complexes (lower two red traces in Figure 2) were much lower in amplitude than the corresponding spectra of the wild type. The most likely explanation for the low amplitudes is that the efficiencies of the S state transitions are substantially decreased by the mutation (i.e., that the "miss" parameter is increased) and that a large fraction of D1-D61A PSII core complexes fails to advance beyond the S_3 state. Typically, spectral features that

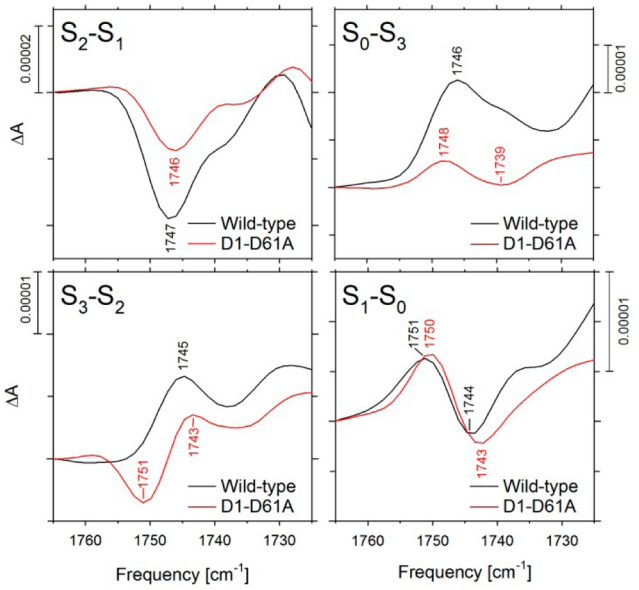

Figure 3. Comparison of the protonated carboxylic acid ν(C=O) regions of the FTIR difference spectra of wild-type (black) and D1-D61A (red) PSII core complexes. The data have been reproduced from Figure 2 but have been shifted vertically to coincide at 1765 cm^{-1}. Note the different vertical scales.

appear in the FTIR difference spectra during the S_1 to S_2 and S_2 to S_3 transitions are reversed during the S_3 to S_0 and S_0 to S_1 transitions.[67−70] If large fractions of the PSII reaction centers fail to advance between S states in response to saturating flashes, PSII reaction centers that undergo the S_3 to S_0 or S_0 to S_1 transitions after the third or fourth flashes may have their spectral features canceled by PSII reaction centers undergoing the S_1 to S_2 or S_2 to S_3 transitions. Consequently, the features in the "S_0-*minus*-S_3" and "S_1-*minus*-S_0" spectra of D1-D61A undoubtedly correspond to a mixture of S state transitions, with the features in the protonated carboxylic acid ν(C=O) region of the "S_1-*minus*-S_0" spectrum (Figure 3, lower right trace) probably corresponding to a reversal of the features observed in the S_2-*minus*-S_1 and S_3-*minus*-S_2 spectra (Figure 3, upper and lower left traces, respectively).

O−H Stretching Region. The O−H stretching vibrations of the weakly H-bonded OH groups of water molecules can be monitored between 3700 and 3500 cm^{-1}.[71,72,75−77,80−88] This region has been examined in the FTIR difference spectra of PSII core complexes from *Thermosynechococcus elongatus*,[82−85] *Synechocystis* sp. PCC 6803,[86,88] and spinach.[87] In our wild-type *Synechocystis* PSII core complexes, this region of the S_2-*minus*-S_1 spectrum shows negative features at 3663 and 3585 cm^{-1} and a weak positive feature at 3616 cm^{-1} (Figure 4, upper left panel, black trace). The corresponding regions of our wild-type S_3-*minus*-S_2, S_0-*minus*-S_3, and S_1-*minus*-S_0 spectra show broad negative features having minima at approximately 3606 cm^{-1}, 3620 cm^{-1}, and 3619 cm^{-1}, respectively (Figure 4, left panels, black traces). If these features correspond to weakly hydrogen-bonded OH groups, they should downshift approximately 900 cm^{-1} in $D_2{}^{16}O$ and approximately 10 cm^{-1} in $H_2{}^{18}O$.[72,82,83] In addition, the features shifted by $D_2{}^{16}O$ should be downshifted further by approximately 17 cm^{-1} by $D_2{}^{18}O$.[72] In Figure 4, the red traces show that the negative features in the "O−H region" downshifted 930−960 cm^{-1} when partly dried samples were moderately hydrated with $D_2{}^{16}O$ (the features vanished from

dx.doi.org/10.1021/bi500309f | *Biochemistry* 2014, 53, 2941−2955

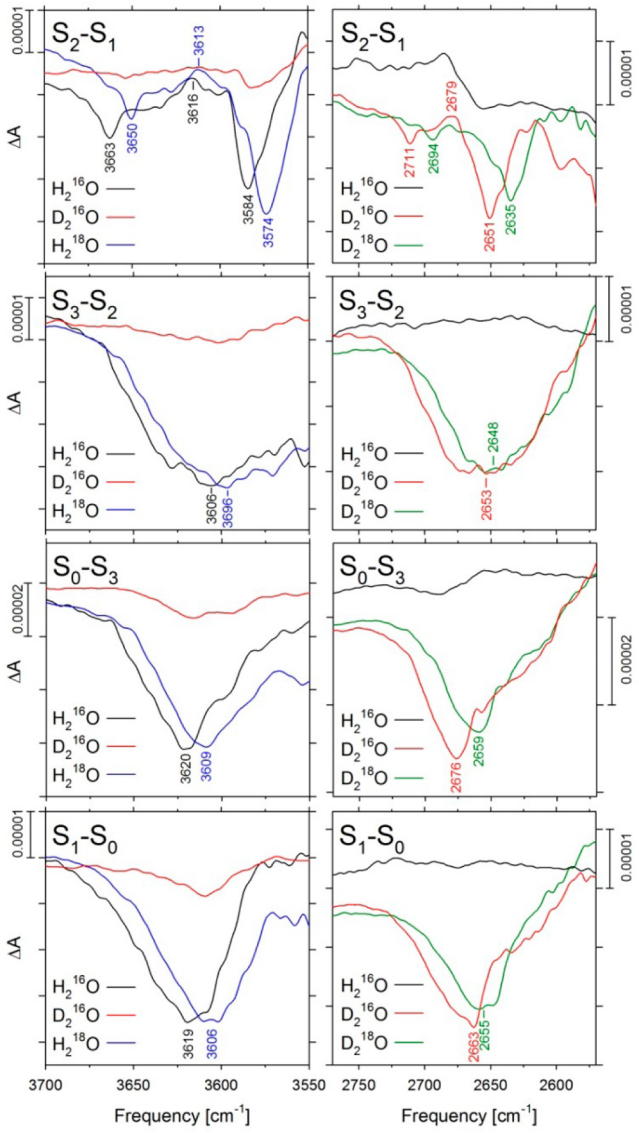

Figure 4. Comparison of the FTIR difference spectra of wild-type PSII core complexes from *Synechocystis* sp. PCC 6803 in the weakly H-bonded O−H stretching region (left panels) and in the weakly D-bonded O−D stretching region (right panels) in response to four successive flash illuminations applied at 0 °C after hydration with $H_2{}^{16}O$ (black), $H_2{}^{18}O$ (blue), $D_2{}^{16}O$ (red), or $D_2{}^{18}O$ (green). The $H_2{}^{16}O$ and $H_2{}^{18}O$ data represent the averages of 14 samples (20,400 scans for each trace) and 16 samples (24,100 scans for each trace), respectively (the $H_2{}^{16}O$ and $H_2{}^{18}O$ data in the left panels are reproduced from ref 88). The $D_2{}^{16}O$ and $D_2{}^{18}O$ data represent the averages of 16 samples (24,000 scans for each trace). Data were normalized to maximize overlap between 1450 and 1350 cm^{-1} and were shifted vertically to coincide approximately at 3700 or 2770 cm^{-1}. Note the different vertical scales.

the 3700−3500 cm^{-1} region and appeared in the "O−D region" between 2700 and 2600 cm^{-1}). The blue traces show that the same features in the 3700−3500 cm^{-1} region downshifted 10−13 cm^{-1} when partly dried samples were moderately hydrated with $H_2{}^{18}O$ (Figure 4, blue traces, left panels). Finally, the green traces show that the features that were downshifted into the "O−D region" by D_2O were further downshifted 5−17 cm^{-1} when partly dried samples were moderately hydrated with $D_2{}^{18}O$ (Figure 4, green traces, right panels). These isotopically induced downshifts confirm that the negative features observed in the 3700−3500 cm^{-1} regions correspond to O−H stretching vibrations that are sensitive to the oxidations of the Mn_4CaO_5 cluster during the S state transitions.[82−84] These regions of the S_{n+1}-*minus*-S_n FTIR difference spectra of D1-D61A PSII core complexes are compared to those of the wild type in Figure 5. This comparison shows that the D1-D61A mutation eliminates the negative feature at 3663 cm^{-1} from the S_2-*minus*-S_1 FTIR spectrum and splits the broad negative feature in the S_3-*minus*-S_2 spectrum into separate minima at 3619 and 3593 cm^{-1}. For the reasons discussed above with respect to the midfrequency spectra of D1-D61A, the spectral features in the O−H region of the "S_0-*minus*-S_3" and "S_1-*minus*-S_0" spectra of D1-D61A probably correspond to a mixture of S state transitions and will not be discussed further here.

D-O-D Bending Region. Because the D-O-D vibrational modes are inherently weak, they are best observed in $D_2{}^{16}O$-*minus*-$D_2{}^{18}O$ double difference spectra.[85] In preparation for calculating these double difference spectra, a comparison of the midfrequency FTIR difference spectra of wild-type PSII core complexes hydrated with $D_2{}^{16}O$ (red) or $D_2{}^{18}O$ (green) is shown in Figure 6. The corresponding comparison of the midfrequency FTIR difference spectra of D1-D61A PSII core complexes hydrated with $D_2{}^{16}O$ (red) or $D_2{}^{18}O$ (green) is shown in Figure 7. To facilitate these comparisons, the data in Figures 6 and 7 are presented with the same vertical scale. The data represent the averages of 16 samples (24,000 scans for each trace) for the wild type and 25−27 samples (37,500−40,500 scans for each trace) for D1-D61A. The figures show the reproducibility of the data employed for calculating the $D_2{}^{16}O$-*minus*-$D_2{}^{18}O$ double difference spectra.

The $D_2{}^{16}O$-*minus*-$D_2{}^{18}O$ double difference spectra of *Synechocystis* sp. PCC 6803 wild-type PSII core complexes in the D-O-D bending [δ(DOD)] region between 1275 and 1125 cm^{-1} in response to four successive flashes are shown in Figure

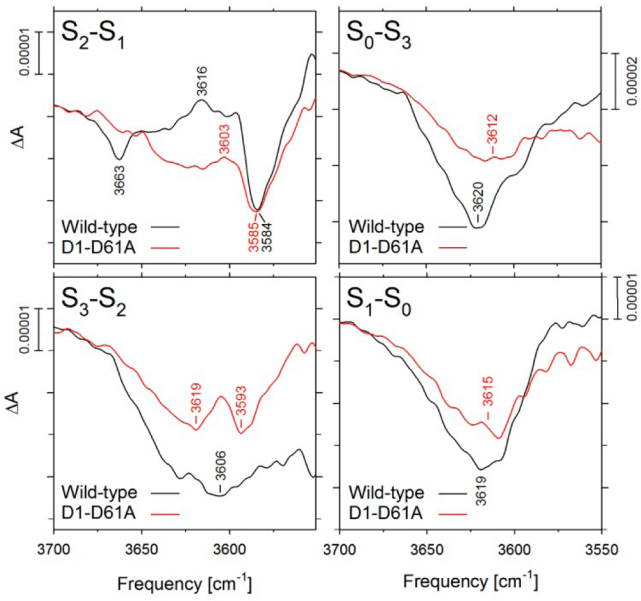

Figure 5. Comparison of the FTIR difference spectra of wild-type (black) and D1-D61A (red) PSII core complexes in the weakly hydrogen bonded O−H stretching region in response to four successive flash illuminations applied at 0 °C. The data were collected simultaneously with that shown in Figure 2, were normalized as in Figure 2, and were shifted vertically to coincide at 3700 cm^{-1}.

dx.doi.org/10.1021/bi500309f | *Biochemistry* 2014, 53, 2941−2955

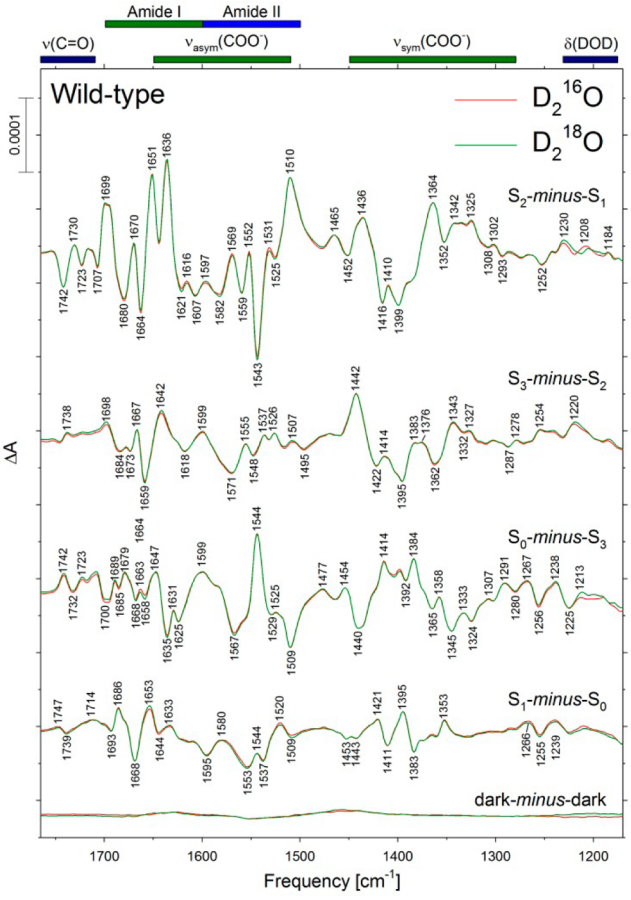

Figure 6. Comparison of the midfrequency FTIR difference spectra of wild-type PSII core complexes in response to four successive flash illuminations applied at 0 °C after hydration with $D_2{}^{16}O$ (red) or $D_2{}^{18}O$ (green). The data represent the averages of 16 samples (24,000 scans for each trace). The data were normalized to maximize overlap with the wild-type spectrum shown in Figure 2. Dark-*minus*-dark control traces are included to show the noise level (lower traces).

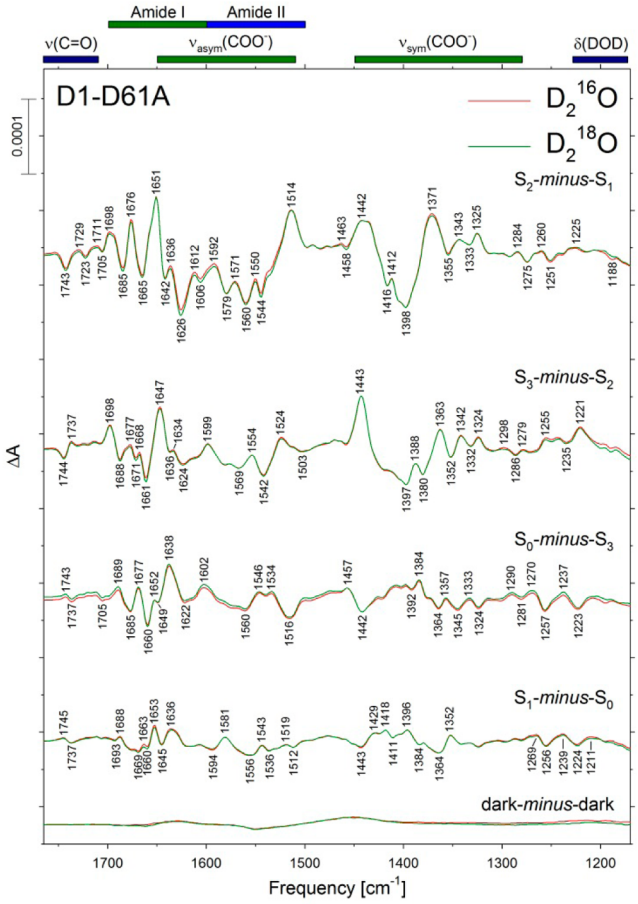

Figure 7. Comparison of the midfrequency FTIR difference spectra of D1-D61A PSII core complexes in response to four successive flash illuminations applied at 0 °C after hydration with $D_2{}^{16}O$ (red) or $D_2{}^{18}O$ (green). The $D_2{}^{16}O$ and or $D_2{}^{18}O$ data represent the averages of 27 samples (40,500 scans for each trace) and 25 samples (37,500 scans for each trace). The data were normalized to maximize overlap with the D1-D61A spectrum shown in Figure 2 and are shown with the same vertical scale used in Figure 6. Dark-*minus*-dark control traces are included to show the noise level (lower traces).

8 (black traces). The corresponding $D_2{}^{16}O$-*minus*-$D_2{}^{18}O$ double difference spectra of D1-D61A PSII core complexes (Figure 8, red traces) show that the mutation eliminates the 1222(−), 1211(+), and 1180(+) features from the S_2-*minus*-S_1 difference spectrum and perturbs some of the features in the S_3-*minus*-S_2 difference spectrum, although most of the features present in the wild-type S_3-*minus*-S_2 spectrum appear to be present in the mutant. For reasons discussed earlier with respect to the midfrequency spectra of D1-D61A, the spectral features in the δ(DOD) region of the "S_0-*minus*-S_3" and "S_1-*minus*-S_0" spectra of D1-D61A probably correspond to a mixture of S state transitions and will not be discussed further here.

Region 3100−2150 cm^{-1}. A comparison of the S_{n+1}-*minus*-S_n FTIR difference spectra of wild-type PSII core complexes between 3100 and 2150 cm^{-1} after hydration with $H_2{}^{16}O$, $H_2{}^{18}O$, $D_2{}^{16}O$, or $D_2{}^{18}O$ is presented in Figure 9 (the region between 3500 and 3100 cm^{-1} is omitted because of the saturating absorption of strongly H-bonded bulk water that is centered near 3300 cm^{-1}[82]). The S_2-*minus*-S_1 spectrum of samples hydrated with $H_2{}^{16}O$ shows many positive features between 3100 and 2600 cm^{-1} (Figure 9, upper left panel, black trace). These features resemble those reported previously in PSII core complexes from *Thermosynechococcus elongatus*.[83,89]

Hydration with $H_2{}^{18}O$ caused no apparent downshifts of any of these features (compare black and blue traces in the top left panel of Figure 9). However, hydration with $D_2{}^{16}O$ diminished the intensities of most of these features as well as that of a broad, underlying feature extending from >3100 cm^{-1} to approximately 2600 cm^{-1} (compare black and red traces in Figure 9). Hydration with $D_2{}^{16}O$ also caused the appearance of several negative features between 2711 and 2559 cm^{-1} and numerous positive features between 2505 and 2186 cm^{-1}. These features also resemble those reported previously in *Thermosynechococcus elongatus* after hydration with $D_2{}^{16}O$.[83] Hydration with $D_2{}^{18}O$ caused no further downshift of the features between 2505 and 2186 cm^{-1} but downshifted the features between 2711 and 2559 cm^{-1} by 13−17 cm^{-1}. The latter features are the weakly D-bonded O−D stretching modes shown in Figure 4 (top right panel) and were discussed above.

The S_3-*minus*-S_2, S_0-*minus*-S_3, and S_1-*minus*-S_0 spectra of samples hydrated with $H_2{}^{16}O$ (Figure 9, lower and right panels) show the presence of broad features centered near 2600 cm^{-1} and extending from approximately 2800 cm^{-1} to approximately 2400 cm^{-1}. These features resemble those reported previously in *Thermosynechococcus elongatus*.[83,89] In *Thermosynechococcus*

dx.doi.org/10.1021/bi500309f | *Biochemistry* 2014, 53, 2941−2955

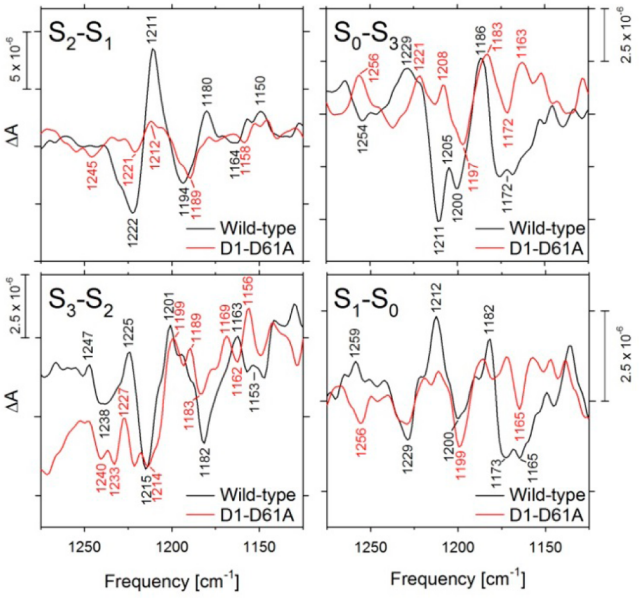

Figure 8. Comparison of the $D_2{}^{16}O$-*minus*-$D_2{}^{18}O$ double difference spectra of wild-type (black) and D1-D61A (red) PSII core complexes between 1275 and 1125 cm^{-1} in response to four successive flashes applied at 0 °C. The data of Figures 6 and 7 were subtracted directly but were offset vertically to maximize overlap. Note the different vertical scales.

elongatus, the broad features are far more prominent than in our data. In our spectra, these features are dwarfed by the features of the D-bonded O−D stretching region that appear in samples hydrated with $D_2{}^{16}O$ or $D_2{}^{18}O$, whereas in *Thermosynechococcus elongatus*, the broad features are larger than the O−D stretching modes.[83]

A comparison of the S_{n+1}-*minus*-S_n FTIR difference spectra of wild-type and D1-D61A PSII core complexes between 3100 and 2150 cm^{-1} is shown in Figure 10. These data show that the mutation eliminated the broad feature extending from >3100 cm^{-1} to approximately 2600 cm^{-1} in the S_2-*minus*-S_1 FTIR difference spectrum of the wild type but not the broad features centered near 2600 cm^{-1} in the S_3-*minus*-S_2, S_0-*minus*-S_3, and S_1-*minus*-S_0 spectra. Most of the features in the spectra of the mutant were diminished in amplitude compared to that of the wild type, as was also observed in the midfrequency and O−H stretching regions (Figures 2 and 5, respectively). Also shown in Figure 10 are the S_2-*minus*-S_1 FTIR difference spectra of D1-D61A after hydration with $D_2{}^{16}O$ (blue) or $D_2{}^{18}O$ (green) between 3100 and 2650 cm^{-1}. These data nearly overlap the S_2-*minus*-S_1 spectrum of D1-D61A hydrated with $H_2{}^{16}O$ (red) between 3000 and 2800 cm^{-1}, confirming the elimination of the broad absorption in the S_2-*minus*-S_1 spectrum by the D1-D61A mutation. For reasons discussed earlier with respect to the midfrequency spectra of D1-D61A, the spectral features of this region of the "S_0-*minus*-S_3" and "S_1-*minus*-S_0" spectra of D1-D61A probably correspond to a mixture of S state transitions and will not be discussed further here.

DISCUSSION

Midfrequency Region. The kinetically efficient transfer of protons through a potential channel requires finely tuned pK_a differences between key residues and the transient formation of clusters of water molecules.[108−111] Consequently, mutation of key residues in a dominant proton egress pathway would be expected to slow the oxidation of the Mn_4CaO_5 cluster in the same manner that mutations that impair proton uptake slow electron transfer from $Q_A^{\bullet-}$ to $Q_B^{\bullet-}$ in reaction centers of *Rhodobacter sphaeroides*[112−114] and the reduction of O_2 to H_2O in cytochrome *c* oxidase.[115−117] A network of hydrogen bonds leading from the Mn_4CaO_5 cluster to the thylakoid lumen via D1-D61 and the D1-E65/D2-E312/D1-R334 triad can been inferred from the distribution of water molecules in the 1.9 Å structural model of PSII.[11,43,44] The mutation of any these four residues,[60,118] or the overdehydration of wild-type samples,[101] substantially decreases the efficiency of the S state transitions. These observations led us to propose that D1-D61, D1-E65, D2-E312, and D1-R334 form part of a dominant proton egress pathway leading from the Mn_4CaO_5 cluster to the lumen.[60,118] The diminished amplitudes of the carboxylate and amide II features at 1586(+), 1552(+), 1543(−), and 1509(+) cm^{-1} in the S_2-*minus*-S_1 FTIR difference spectrum of D1-D61A PSII core complexes (Figure 2, top red trace) are also observed in overly dehydrated samples[60] and in PSII core complexes from D1-E65A, D2-E312Q, and D1-R334A.[60,118] These spectral changes may reflect similar perturbations of the polypeptide backbone that are caused by the disruption of a common network of hydrogen bonds. The 1530(+)/1522(−) cm^{-1} feature in the wild-type S_2-*minus*-S_1 FTIR difference spectrum that is eliminated by the D1-D61A mutation (Figure 2, top red trace) is also eliminated by the D2-E312A[60] and D1-R334A[118] mutations and by mutations of residues that coordinate the nearby $Cl^-(1)$ ion, such as D2-K317A[107] and D1-N181A (not shown). The elimination of the same feature by mutations constructed at D1-D61, D1-N181, D1-R334, D2-E312, and D2-K317 suggests the partial disruption of a common network of hydrogen bonds that includes D1-D61 and the $Cl^-(1)$ ion.

We recently concluded that the features observed in the protonated carboxylic acid ν(C=O) regions of the S_{n+1}-*minus*-S_n FTIR difference spectra of wild-type PSII core complexes from *Synechocystis* sp. PCC 6803 arise from three separate carboxylic acid groups.[118] The pK_a value of one decreases in response to the increased charge that develops on the Mn_4CaO_5 cluster during the S_1 to S_2 transition, giving rise to the negative 1747 cm^{-1} feature in the S_2-*minus*-S_1 FTIR difference spectrum. This feature is diminished or eliminated by overdehydration of samples or by the mutations D1-E65A, D2-E312A, D1-E329Q, and D1-R334A, providing evidence for an extensive network of hydrogen bonds that extends at least 20 Å across the lumenal face of the Mn_4CaO_5 cluster.[60,118] In the current study, we find that the D1-D61A mutation substantially decreases the amplitude of the 1747(−) cm^{-1} feature, providing evidence that D1-D61 participates in the same network of hydrogen bonds, as is expected on the basis of the 1.9 Å structural model.[11,12] The pK_a value of a second carboxylic acid group *increases* in response to the changes in the Mn_4CaO_5 cluster's geometry that occur during the S_2 to S_3 transition, giving rise to the positive 1745 cm^{-1} feature in the S_3-*minus*-S_2 FTIR difference spectrum.[118] This feature is eliminated by the mutations D1-Q165E and D1-E329Q, providing evidence for an additional network of hydrogen bonds that extends at least 13 Å across the face of the Mn_4CaO_5 cluster opposite from the D1-E65/D2-E313/D1-R334 triad. As noted previously,[118] because D1-E329 also participates in the network of hydrogen bonds that includes the D1-E65/D2-E312/D1-R334 triad, the complete, combined network must be quite extensive, although some elements may exist only transiently. In the current work, we find that the D1-D61A mutation alters the 1745(+) cm^{-1}

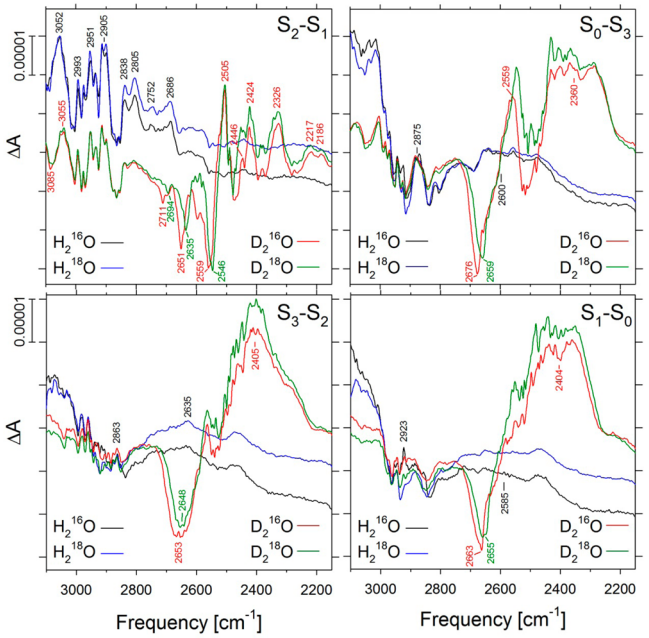

Figure 9. Comparison of the S_{n+1}-*minus*-S_n FTIR difference spectra of wild-type PSII core complexes from *Synechocystis* sp. PCC 6803 between 3100 and 2150 cm^{-1} in response to four successive flash illuminations applied at 0 °C after hydration with $H_2{}^{16}O$ (black), $H_2{}^{18}O$ (blue), $D_2{}^{16}O$ (red), or $D_2{}^{18}O$ (green). Data were normalized to maximize overlap between 1450 and 1350 cm^{-1}.

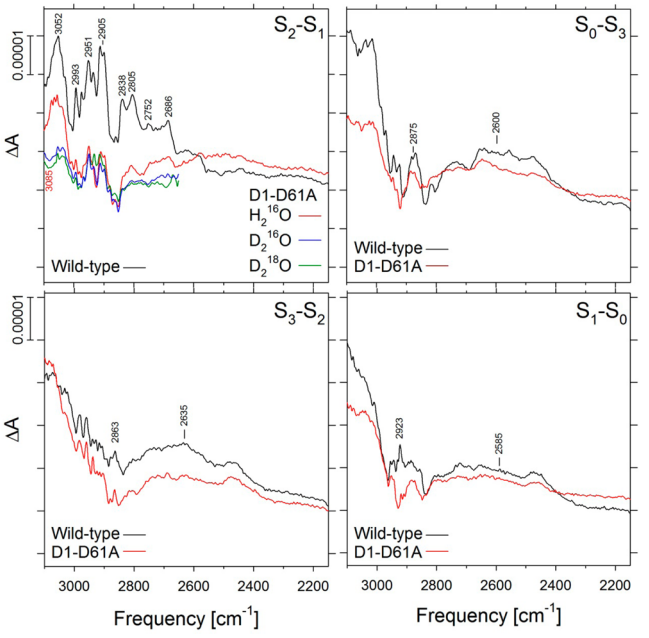

Figure 10. Comparison of the FTIR difference spectra of wild-type (black) and D1-D61A (red) PSII core complexes between 3100 and 2150 cm^{-1} in response to four successive flash illuminations applied at 0 °C. The data in the upper left panel include the S_2-*minus*-S_1 FTIR difference spectra of D1-D61A between 3100 and 2650 cm^{-1} after hydration with $D_2{}^{16}O$ (blue) or $D_2{}^{18}O$ (green). The data were collected simultaneously with that shown in Figure 2, were normalized as in Figure 2, and were shifted vertically to coincide at 3700 cm^{-1}.

feature, providing evidence that D1-D61 also participates in the network of hydrogen bonds that extends to D1-Q165.

O−H Stretching Region. In PSII core complexes from *Thermosynechococcus elongatus*[82−84] and spinach,[87] the S_2-*minus*-S_1 FTIR difference spectrum exhibits a derivative-shaped feature having a negative peak at 3585−3588 cm^{-1} and a positive peak at 3613−3618 cm^{-1}. This feature has been attributed to a water molecule coupled to the Mn_4CaO_5 cluster and having an asymmetric hydrogen-bonding structure in the S_1 state and an even greater asymmetry of hydrogen-bonding in the S_2 state.[82−84] In our wild-type *Synechocystis* S_2-*minus*-S_1 difference spectrum (Figure 4, upper left panel), the negative and positive peaks appear at 3584 and 3616 cm^{-1} respectively, with the positive peak being less distinct than that in *Thermosynechococcus elongatus* or spinach [similar data have been reported previously for *Synechocystis* sp. PCC 6803,[86] but the difference with *Thermosynechococcus elongatus* was not mentioned]. Our spectrum contains a negative feature at 3663 cm^{-1} that we reported previously.[88] Only a very weak vestige of this feature has been observed in *Thermosynechococcus elongatus*,[82,83] and it has not been reported in spinach.[87] The greater prominence of this feature in our samples might be caused by the higher hydration of our samples (99% relative humidity) compared to those examined previously by others. The extent of sample hydration is known to substantially affect the amplitudes of features in the S_{n+1}-*minus*-S_n FTIR difference spectra.[60,101,119]

In *Thermosynechococcus elongatus*, the S_3-*minus*-S_2, S_0-*minus*-S_3, and S_1-*minus*-S_0 difference spectra exhibit broad negative features having minima at 3634, 3621, and 3612 cm^{-1}, respectively.[83,84] These features have been attributed to water molecules or hydroxide groups that are located on or near the Mn_4CaO_5 cluster and that either deprotonate or form stronger hydrogen bonds (i.e., weakly hydrogen-bonded OH groups become strongly hydrogen-bonded) during the S_2 to S_3, S_3 to S_0, and S_0 to S_1 transitions.[83,84] Accordingly, we assign the negative feature at 3663 cm^{-1} observed in the wild-type S_2-*minus*-S_1 FTIR difference spectrum to a water molecule or hydroxide group on or near the Mn_4CaO_5 cluster that either deprotonates or forms a stronger hydrogen bond during the S_1 to S_2 transition. In our spectra of wild-type *Synechocystis* sp. PCC 6803, the minima of the S_3-*minus*-S_2 and S_1-*minus*-S_0 spectra are shifted from those observed with *Thermosynechococcus elongatus*, particularly the minimum in the S_3-*minus*-S_2 spectrum. These shifts may reflect slight differences between the networks of hydrogen bonds around the Mn_4CaO_5 cluster in the two species of cyanobacteria.

The D1-D61A mutation eliminates the negative feature at 3663 cm^{-1} from the S_2-*minus*-S_1 spectrum and splits the broad negative feature in the S_3-*minus*-S_2 spectrum into separate minima at 3619 and 3593 cm^{-1}. Because the negative feature at 3663 cm^{-1} corresponds to a water molecule or hydroxide group on or near the Mn_4CaO_5 cluster that either deprotonates or forms a stronger hydrogen bond during the S_1 to S_2 transition, we conclude that the hydrogen-bonding properties of this water molecule or hydroxide group are altered by the mutation. This negative feature is also eliminated by the D1-E333Q[88] and D2-K317A (not shown) mutations but not by the D1-D170H mutation (not shown), suggesting that the group in question may be a water molecule located near the $Cl^-(1)$ ion. The split of the broad negative feature in the S_3-*minus*-S_2 spectrum into two separate minima is unique to D1-D61A, suggesting that at least some of the water molecules/hydroxide groups deprotonating or forming stronger hydrogen bonds during the S_2 to S_3 transition are located near D1-D61.

dx.doi.org/10.1021/bi500309f | *Biochemistry* 2014, 53, 2941−2955

D-O-D Bending Region. Our $D_2{}^{16}O$-*minus*-$D_2{}^{18}O$ double difference spectra resemble those reported previously for *Thermosynechococcus elongatus*,[85] especially the 1222(−)/1211(+)/1194(−)/1180(+) cm^{-1} features in the S_2-*minus*-S_1 spectrum, the 1238(−)/1225(+)/1215(−)/1201(+)/1182(−) cm^{-1} features in the S_3-*minus*-S_2 spectrum, the 1211(−)/1205(+)/1200(−)/1186(+) cm^{-1} features in the S_0-*minus*-S_3 spectrum, and the 1229(−)/1212(+)/1200(−)/1182(+) cm^{-1} features in the S_1-*minus*-S_0 spectrum, nearly all of which correspond to those in the corresponding *Thermosynechococcus elongatus* spectra within 3 cm^{-1}. One important observation corresponding with the *T. elongatus* data is that the amplitudes of several of these peaks oscillate during the S state transitions. For example, the large positive feature at 1211 cm^{-1} in the S_2-*minus*-S_1 spectrum is negative (at 1211−1215 cm^{-1}) in the S_3-*minus*-S_2 and S_0-*minus*-S_3 spectra and positive again in the S_1-*minus*-S_0 spectrum. Other examples are the peak at 1222−1229 cm^{-1} (negative in the S_2-*minus*-S_1 and S_1-*minus*-S_0 spectra and positive in the S_3-*minus*-S_2 and S_0-*minus*-S_3 spectra) and at 1182 cm^{-1} (positive in the S_2-*minus*-S_1 spectrum and negative in the S_3-*minus*-S_2 spectrum). These oscillations imply that some of the δ(DOD) alterations are reversed during the S state cycle. Another important observation is that the negative features at 1238 cm^{-1} in the S_3-*minus*-S_2 spectrum and at and 1254 cm^{-1} in the S_0-*minus*-S_3 spectrum have no apparent positive counterparts in the other spectra. Similar features (at 1235 and 1242 cm^{-1}, respectively) were observed in these spectra in *Thermosynechococcus elongatus*[85] and attributed to substrate water molecules that insert into the Mn_4CaO_5 cluster from a cluster of water molecules within PSII during the S_2 to S_3 and S_3 to S_0 transitions.[85] The small differences between our spectra and those of *Thermosynechococcus elongatus*[85] are probably caused by slight differences in the networks of hydrogen bonds around the Mn_4CaO_5 cluster in the two species of cyanobacteria.

In a $D_2{}^{16}O$-*minus*-$D_2{}^{18}O$ double difference spectrum, the alteration of a single D-O-D bending vibration during an S state transition will cause four peaks to appear (two from $D_2{}^{16}O$ and two from $D_2{}^{18}O$). In contrast, if a D_2O molecule deprotonates during a transition, the bending mode will disappear, and only two peaks will appear in the double difference spectrum. One complication is that some positive and negative peaks may overlap and cancel their intensities, decreasing the number of bands observed. In our data, at least four bands are observed in each double difference spectrum, implying that one or two D_2O molecules have their D-O-D bending modes altered during each S state transition. These D_2O molecules likely reside in the first or second coordination sphere of the Mn_4CaO_5 cluster or in a nearby network of hydrogen bonds. The D1-D61A mutation eliminates the 1222(−), 1211(+), and 1180(+) features from the $D_2{}^{16}O$-*minus*-$D_2{}^{18}O$ double difference spectrum of the S_1 to S_2 transition. It seems reasonable to conclude that one of the D_2O molecules whose δ(DOD) mode changes in response to the positive charge that develops on the Mn_4CaO_5 cluster during the S_1 to S_2 transition is no longer present in the mutant and that this D_2O molecule forms a hydrogen bond to D1-D61 in wild-type PSII (Figure 1). The perturbation of the network of hydrogen bonds caused by the absence of this D_2O molecule in D1-D61A PSII core complexes may cause the alterations to the $D_2{}^{16}O$-*minus*-$D_2{}^{18}O$ double difference spectrum of the S_2 to S_3 transition (Figure 8, lower left trace). The absence of this H_2O molecule in D1-D61A may also impede proton egress from the Mn_4CaO_5 cluster, thereby contributing to the decreased efficiency of the S state transitions in this mutant. Most of the features that are present in the $D_2{}^{16}O$-*minus*-$D_2{}^{18}O$ double difference spectrum of the S_2 to S_3 transition in wild-type PSII appear to be present in the spectrum of the mutant. Consequently, it seems likely that the D_2O molecules whose δ(DOD) mode changes in response to the alterations in the Mn_4CaO_5 cluster's geometry that occur during the S_2 to S_3 transition do not interact directly with D1-D61.

Region 3100−2150 cm^{-1}. A broad feature centered at 3000 cm^{-1} in the S_2-*minus*-S_1 FTIR difference spectrum of PSII core complexes from *Thermosynechococcus elongatus* was assigned previously to changes in the polarization of a highly polarized network of strong hydrogen bonds (known as Zundel polarizability) near the Mn_4CaO_5 cluster.[83,89] Similar broad features in the S_3-*minus*-S_2, S_0-*minus*-S_3, and S_1-*minus*-S_0 spectra, centered at 2700, 2550, and 2600 cm^{-1}, respectively, were assigned to the same origin.[83,89] These features were sharply diminished or eliminated by hydration with $D_2{}^{16}O$.[83] The higher frequency of the features in the S_2-*minus*-S_1 spectrum was attributed to the Mn_4CaO_5 cluster's lack of deprotonation during the S_1 to S_2 transition: compared to the other S state transitions, the extra proton would strengthen the hydrogen-bond network, providing lower frequency features. We confirm these broad features in our S_{n+1}-*minus*-S_n FTIR difference spectra of this region, although in our spectra these features are dominated by the much larger features of the D-bonded O−D stretching region. Although we confirm that hydration with $D_2{}^{16}O$ diminishes the broad feature in the S_2-*minus*-S_1 spectrum, the dominance of the O−D stretching modes prevented us from confirming that the broad features in the other S_{n+1}-*minus*-S_n are diminished by hydration with $D_2{}^{16}O$ or $D_2{}^{18}O$.

The D1-D61A mutation eliminates the broad feature from the S_2-*minus*-S_1 FTIR difference spectrum of the wild type. Its absence from the S_2-*minus*-S_1 FTIR difference spectrum of the mutant was confirmed by the similarity of the mutant spectrum (hydrated with $H_2{}^{16}O$) to the spectrum of the mutant after hydration with $D_2{}^{16}O$ or $D_2{}^{18}O$: evidently, no broad feature remained in the mutant to be eliminated by deuteration. We conclude that the highly polarizable network of hydrogen bonds whose polarizability or protonation state increases during the S_1 to S_2 transition involves D1-D61. Because the broad feature centered near 2600 cm^{-1} in the wild-type S_3-*minus*-S_2 spectrum remained present in the mutant (albeit with a lower amplitude), we conclude that the highly polarizable network of hydrogen bonds whose polarizability or protonation state increases during the S_2 to S_3 transition does not include D1-D61.

It was reported recently that a substrate-containing cluster of five water molecules accepts a proton from the Mn_4CaO_5 cluster during the S_1 to S_2 transition.[90] This conclusion was based on the analysis of a broad positive feature at 2880 cm^{-1} in the S_2-*minus*-S_1 FTIR difference spectra of Ca^{2+}-reconstituted spinach PSII core complexes. This feature undoubtedly corresponds to the broad feature in the S_2-*minus*-S_1 FTIR difference spectrum reported in refs 83 and 89 and in the current study. In ref 90, this feature was eliminated by a variety of treatments including exchange of $H_2{}^{16}O$ for $D_2{}^{16}O$, extraction of Ca^{2+}, replacement of Ca^{2+} with Sr^{2+} or Mg^{2+}, and treatment with ammonia. However, the spectrum of Ca^{2+}-reconstituted PSII presented in ref 90 lacks many of the features that are present in the corresponding S_2-*minus*-S_1 FTIR

difference spectrum of *Thermosynechococcus elongatus*[83,89,120] and in the current study. In addition, the spectrum in ref 90 is essentially featureless after the exchange of $H_2{}^{16}O$ for $D_2{}^{16}O$, in contrast to the corresponding spectra reported in ref 83 and in the current study. In agreement with refs 83 and 89, we confirm that a wealth of features overlay the broad feature in the S_2-*minus*-S_1 spectrum. These overlying features do not correspond to the O−H stretching vibrations of water molecules because they do not downshift after hydration with $H_2{}^{18}O$. They have been attributed to a mixture of C−H stretching vibrations from aliphatic groups and N−H stretching vibrations and their Fermi resonance overtones from the imidazole group(s) of one or more histidine residues.[82,83,120] The N−H stretching vibrations are expected to downshift 500−700 cm^{-1} in the presence of $D_2{}^{16}O$.[78,121] Consequently, the diminished amplitudes of the positive features at 3052, 2993, 2951, and 2905 cm^{-1} in our data may reflect the $D_2{}^{16}O$-induced shifts of parts of these features to 2505, 2446, 2424, and 2326 cm^{-1}, respectively, with the remaining features at 3052, 2993, 2951, and 2905 cm^{-1} corresponding to C−H stretching modes. Importantly, most of these features are missing from the S_2-*minus*-S_1 difference spectrum of Ca^{2+}-reconstituted PSII presented in ref 90, especially after the exchange of $H_2{}^{16}O$ for $D_2{}^{18}O$, in contrast to the data presented in refs 83 and 89 and in the current study. Furthermore, the authors of ref 90 presented no midfrequency FTIR difference spectra other than a schematic illustration of the S_2-*minus*-S_1 spectrum of presumably untreated spinach PSII core complexes. This omission makes it impossible for the reader to independently assess the quality of most of the data presented in ref 90 because there is no means of assessing the quality of the treated samples (i.e., the samples depleted of Ca^{2+}, having Ca^{2+} replaced with Sr^{2+} or Mg^{2+}, or treated with ammonia) after being dried onto the FTIR windows. This omission also makes it impossible to independently assess the extent to which advancement to the S_3 or S_0 states was achieved in response to the appropriate number of actinic flashes (the authors do not report rehydrating their dried FTIR samples; rehydration of dried FTIR samples to a relative humidity of at least 95% is critical for efficient S state cycling[101]). One particular concern is the similarity of the S_3-*minus*-S_2, S_0-*minus*-S_3, and S_1-*minus*-S_0 spectra in Ca^{2+}-reconstituted PSII reported in ref 90: they are all reported to be dominated by the same broad negative feature at 2820 cm^{-1}. In contrast, the corresponding spectra presented in refs 83 and 89 and in the current study show differences between the S_3-*minus*-S_2, S_0-*minus*-S_3, and S_1-*minus*-S_0 spectra in this region. Also, the authors of ref 90 attributed the negative features near 2880 cm^{-1} in their S_3-*minus*-S_2, S_0-*minus*-S_3, and S_1-*minus*-S_0 spectra to the deprotonation of a cationic water cluster during the S_2 to S_3, S_3 to S_0, and S_0 to S_1 transitions. However, no $H_2{}^{16}O/D_2{}^{16}O$ exchange data were presented to support the assignment of these features to vibrational modes of water molecules. In *Thermosynechococcus elongatus*[83] and in the current study, the features near 2900 cm^{-1} in the S_3-*minus*-S_2, S_0-*minus*-S_3, and S_1-*minus*-S_0 spectra are largely insensitive to hydration with $D_2{}^{16}O$. Instead, $D_2{}^{16}O$-sensitive positive features centered at 2700, 2550, and 2600 cm^{-1} were reported.[83] We confirm these features in the current study. These features were not observed in ref 90 as pointed out by the authors and demonstrated in their Figure S3. Finally, the spectra of the weakly H-bonding O−H stretching region presented in ref 90 (between 3700 and 3500 cm^{-1}) contained no reproducible features above the baseline, as was also pointed out by the authors and also demonstrated in their Figure S3. In contrast, reproducible spectral features in this region have been presented by several laboratories in PSII core complexes isolated from *Thermosynechococcus elongatus*,[82−84] *Synechocystis* sp. PCC 6803[86,88] (and the current study), and spinach.[87]

Broad features in the 3000−2000 cm^{-1} region that are sensitive to H_2O/D_2O exchange suggest the existence of one or more delocalized protons in a highly polarizable network of hydrogen bonds made up of amino acid side chains and water molecules.[74,75,78−80,83] The polarizability is caused by the fluctuations of protons within the network of hydrogen bonds. The extreme breadth of the features is caused by strong interactions between the fluctuating protons and local electrostatic fields. The broad features that appear in all of the S_{n+1}-*minus*-S_n spectra in refs 83 and 89 and in the current study all have *positive* amplitudes. The positive amplitudes imply that the concentration and/or the polarizability of the protons in the network increases during each S state transition. It remains unclear whether the broad features originate from an increase of the polarizability of the protons in the network, from increased protonation of the network, or from a combination of both effects. Because the broad feature in the S_2-*minus*-S_1 spectrum is centered at a higher frequency than the features in the other transitions, a different combination of effects may take place during the S_1 to S_2 transition and may be related to the development of positive charge on the Mn_4CaO_5 cluster that is believed to accompany this transition on the basis of a variety of measurements.[122−132] The recent conclusion that a broad feature at 2880 cm^{-1} corresponds to a substrate-containing cluster of five water molecules that accepts a proton from the Mn_4CaO_5 cluster during the S_1 to S_2 transition and that deprotonates during the subsequent S state transitions[90] needs to be reassessed.

SUMMARY AND CONCLUSIONS

The D1-D61A mutation substantially decreases the amplitudes of the 1747(−)cm^{-1} feature in the S_2-*minus*-S_1 FTIR difference spectrum and alters the appearance of the 1745(+) cm^{-1} feature in the S_3-*minus*-S_2 FTIR difference spectrum, providing additional experimental evidence that D1-D61 participates the same extensive networks of hydrogen bonds identified previously as extending across the Mn_4CaO_5 cluster. The D1-D61A mutation eliminates the same negative feature at 3663 cm^{-1} from the S_2-*minus*-S_1 difference spectrum as several other mutations, suggesting that this feature corresponds to a water molecule or hydroxide group located near the $Cl^-(1)$ ion. The D1-D61A mutation also splits the broad negative feature that appears near 3606 cm^{-1} in the S_3-*minus*-S_2 difference spectrum into two separate minima, suggesting that these features correspond to water molecules or hydroxide groups located near D1-D61. The elimination by the D1-D61A mutation of the 1222(−), 1211(+), and 1180(+) features from the S_2-*minus*-S_1 $D_2{}^{16}O$-*minus*-$D_2{}^{18}O$ double difference spectrum suggests that D1-D61 forms a hydrogen bond to one of the H_2O molecules whose δ(HOH) mode changes in response to the S_1 to S_2 transition. The elimination of this H_2O molecule in the D1-D61A mutant provides one rationale for the decreased efficiency of the water oxidation in this mutant. Finally, the elimination by the D1-D61A mutation of the broad positive feature centered near 2900 cm^{-1} in the S_2-*minus*-S_1 difference spectrum shows that the highly polarizable network of hydrogen bonds whose polarizability or protonation state increases during the S_1 to S_2 transition involves D1-D61. It

remains an open question whether the broad positive features observed in the S_{n+1}-*minus*-S_n FTIR difference spectra between 3000 and 2200 cm^{-1}, first observed by Noguchi and co-workers in 2002 and attributed to delocalized protons in a highly polarizable network of hydrogen bonds near the Mn_4CaO_5 cluster, originate from increased polarizability of the protons in this network or from increased protonation of this network during each S state transition.

AUTHOR INFORMATION

Corresponding Author

*Phone: 951-27-3483. Fax: 951-827-4294. E-mail: richard.debus@ucr.edu.

Funding

This work was supported by the Department of Energy, Office of Basic Energy Sciences, Division of Chemical Sciences (grant DE-FG02-10ER16191).

Notes

The authors declare no competing financial interest.

ACKNOWLEDGMENTS

I am grateful to Anh P. Nguyen for maintaining the mutant and wild-type cultures of *Synechocystis* sp. PCC 6803 and for purifying the thylakoid membranes that were used for the isolation of PSII core complexes and to Takumi Noguchi for helpful discussions.

DEDICATION

This article is dedicated to the memory of Warwick Hillier (October 18, 1967 to January 10, 2014), a dear friend and colleague who taught me how to obtain FTIR spectra.

ABBREVIATIONS

Chl, chlorophyll; DCMU, 3-(3,4-dichlorophenyl)-1,1-dimethylurea; EDTA, ethylenediaminetetraacetic acid; EPR, electron paramagnetic resonance; EXAFS, extended X-ray absorption fine structure; FTIR, Fourier transform infrared; MES, 2-(*N*-morpholino)-ethanesulfonic acid; NTA, nitrilotriacetic acid; P_{680}, chlorophyll multimer that serves as the light-induced electron donor in PSII; Pheo, pheophytin; PSII, photosystem II; Q_A, primary plastoquinone electron acceptor; Q_B, secondary plastoquinone electron acceptor; XANES, X-ray absorption near edge structure; Y_Z, tyrosine residue that mediates electron transfer between the Mn_4Ca cluster and $P_{680}^{+\bullet}$

REFERENCES

(1) Cardona, T., Sedoud, A., Cox, N., and Rutherford, A. W. (2012) Charge separation in Photosystem II: A comparative and evolutionary overview. *Biochim. Biophys. Acta 1817*, 26−43.

(2) Barber, J. (2012) Photosystem II: The Water-Splitting Enzyme of Photosynthesis. *Cold Spring Harbor Symp. Quant. Biol. 77*, 295−307.

(3) Shi, L.-X., Hall, M., Funk, C., and Schröder, W. P. (2012) Photosystem II, a growing complex: Updates on newly discovered components and low molecular mass proteins. *Biochim. Biophys. Acta 1817*, 13−25.

(4) Vinyard, D. J., Ananyev, G. M., and Dismukes, G. C. (2013) Photosystem II: the reaction center of oxygenic photosynthesis. *Annu. Rev. Biochem. 82*, 577−606.

(5) Messinger, J., Noguchi, T., and Yano, J. (2012) Photosynthetic O_2 Evolution, in *Molecular Solar Fuels* (Wydrzynski, T. and Hillier, W., Eds.) pp 163−207, Royal Society of Chemistry, Cambridge, UK.

(6) Renger, G. (2012) Mechanism of light induced water splitting in Photosystem II of oxygen evolving photosynthetic organisms. *Biochim. Biophys. Acta 1817*, 1164−1176.

(7) Dau, H., Zaharieva, I., and Haumann, M. (2012) Recent developments in research on water oxidation by photosystem II. *Curr. Opin. Chem. Biol. 16*, 3−10.

(8) Cox, N., Pantazis, D. A., Neese, F., and Lubitz, W. (2013) Biological water oxidation. *Acc. Chem. Res. 46*, 1588−1596.

(9) Cox, N., and Messinger, J. (2013) Reflections on substrate water and dioxygen formation. *Biochim. Biophys. Acta 1827*, 1020−1030.

(10) Pokhrel, R., and Brudvig, G. W. (2014) Oxygen-evolving complex of photosystem II: correlating structure with spectroscopy. *Phys. Chem. Chem. Phys.*, DOI: 10.1039/C4CP00493K.

(11) Umena, Y., Kawakami, K., Shen, J.-R., and Kamiya, N. (2011) Crystal structure of oxygen-evolving Photosystem II at a resolution of 1.9 Å. *Nature 473*, 55−60.

(12) Kawakami, K., Umena, Y., Kamiya, N., and Shen, J.-R. (2011) Structure of the catalytic, inorganic core of oxygen-evolving Photosystem II at 1.9 Å resolution. *J. Photochem. Photobiol., B 104*, 9−18.

(13) Luber, S., Rivalta, I., Umena, Y., Kawakami, K., Shen, J.-R., Kamiya, N., Brudvig, G. W., and Batista, V. S. (2011) S_1-state model of the O_2-evolving complex of Photosystem II. *Biochemistry 50*, 6308−6311.

(14) Ames, W., Pantazis, D. A., Krewald, V., Cox, N., Messinger, J., Lubitz, W., and Neese, F. (2011) Theoretical evaluation of structural models of the S_2 state in the oxygen evolving complex of Photosystem II: protonation states and magnetic interactions. *J. Am. Chem. Soc. 133*, 19743−19757.

(15) Siegbahn, P. E. M. (2011) The effect of backbone constraints: the case of water oxidation by the oxygen-evolving complex in PSII. *ChemPhysChem 12*, 3274−3280.

(16) Kusunoki, M. (2011) S_1-state Mn_4Ca complex of Photosystem II exists in equilibrium between the two most-stable isomeric substates: XRD and EXAFS evidence. *J. Photochem. Photobiol., B 104*, 100−110.

(17) Galstyan, A., Robertazzi, A., and Knapp, E. W. (2012) Oxygen-evolving Mn cluster in Photosystem II: the protonation pattern and oxidation state in the high-resolution crystal structure. *J. Am. Chem. Soc. 134*, 7442−7449.

(18) Isobe, H., Shoji, M., Yamanaka, S., Umena, Y., Kawakami, K., Kamiya, N., Shen, J.-R., and Yamaguchi, K. (2012) Theoretical illumination of water-inserted structures of the $CaMn_4O_5$ cluster in the S_2 and S_3 states of oxygen-evolving complex of photosystem II: full geometry optimizations by B3LYP hybrid density functional. *Dalton Trans. 41*, 13727−13740.

(19) Siegbahn, P. E. M. (2009) Structures and energetics for O_2 formation in Photosystem II. *Acc. Chem. Res. 42*, 1871−1880.

(20) Yamanaka, S., Isobe, H., Kanda, K., Saito, T., Umena, Y., Kawakami, K., Shen, J.-R., Kamiya, N., Okamura, M., Nakamura, H., and Yamaguchi, K. (2011) Possible mechanisms for the O-O bond formation in oxygen evolution reaction at the $CaMn_4O_5(H_2O)_4$ cluster of PSII refined to 1.9 Å resolution. *Chem. Phys. Lett. 511*, 138−145.

(21) Siegbahn, P. E. M. (2012) Mechanisms for proton release during water oxidation in the S_2 to S_3 and S_3 to S_4 transitions in photosystem II. *Phys. Chem. Chem. Phys. 14*, 4849−4856.

(22) Rapatskiy, L., Cox, N., Savitsky, A., Ames, W. M., Sander, J., Nowaczyk, M. M., Rögner, M., Boussac, A., Neese, F., Messinger, J., and Lubitz, W. (2012) Detection of water-binding sites of the oxgyen-evolving complex of Photosystem II using W-band ^{17}O electron-electron double resonance-detected NMR spectroscopy. *J. Am. Chem. Soc. 134*, 16619−16634.

(23) Siegbahn, P. E. M. (2013) Water oxidation mechanism in photosystem II, including oxidations, proton release pathways, O-O bond formation and O_2 release. *Biochim. Biophys. Acta 1827*, 1003−1019.

(24) Siegbahn, P. E. M. (2013) Substrate water exchange of the oxygen evolving complex in PSII in the S_1, S_2, and S_3 states. *J. Am. Chem. Soc. 135*, 9442−9449.

(25) Navarro, M. P., Ames, W. M., Nilsson, H., Lohmiller, T., Pantazis, D. A., Rapatskiy, L., Nowaczyk, M. M., Neese, F., Boussac, A., Messinger, J., Lubitz, W., and Cox, N. (2013) Ammonia binding to the oxygen-evolving complex of photosystem II identified the solvent-exchangeable oxygen bridge (μ-oxo) of the manganese tetramer. *Proc. Natl. Acad. Sci. U.S.A. 110*, 15561−15566.
(26) Pantazis, D. A., Ames, W., Cox, N., Lubitz, W., and Neese, F. (2012) Two interconvertable structures that explain the spectroscopic properties of the oxygen-evolving complex of Photosystem II in the S_2 state. *Angew. Chem., Int. Ed. 51*, 9935−9940.
(27) Saito, K., and Ishikita, H. (2013) Influence of the Ca^{2+} ion on the Mn_4Ca conformation and the H-bond network arrangement in Photosystem II. *Biochim. Biophys. Acta 1837*, 159−166.
(28) Bovi, D., Narzi, D., and Guidoni, L. (2013) The S_2 state of the oxygen-evolving complex of Photosystem II explored by QM/MM dynamics: spin surfaces and metastable states suggest a reaction path towards the S_3 state. *Angew. Chem., Int. Ed. 52*, 11744−11749.
(29) Glöckner, C., Kern, J., Broser, M., Zouni, A., Yachandra, V. K., and Yano, J. (2013) Structural changes of the oxygen-evolving complex in Photosystem II during the catalytic cycle. *J. Biol. Chem. 288*, 22607−22620.
(30) McEvoy, J. P., and Brudvig, G. W. (2006) Water-splitting chemistry of Photosystem II. *Chem. Rev. 106*, 4455−4483.
(31) Dau, H., and Haumann, M. (2007) Eight steps preceding O-O bond formation in oxygenic photosynthesis - A basis reaction cycle of the Photosystem II manganese complex. *Biochim. Biophys. Acta 1767*, 472−483.
(32) Dau, H., and Haumann, M. (2008) The manganese complex of Photosystem II in its reaction cycle - basic framework and possible realization at the atomic level. *Coord. Chem. Rev. 252*, 273−295.
(33) Sproviero, E. M., Gascón, J. A., McEvoy, J. P., Brudvig, G. W., and Batista, V. S. (2008) Quantum mechanics/molecular mechanics study of the catalytic cycle of water splitting in Photosystem II. *J. Am. Chem. Soc. 130*, 3428−3442.
(34) Dau, H., Limberg, C., Reier, T., Risch, M., Roggan, S., and Strasser, P. (2010) The mechanism of water oxidation: from electrolysis via homogeneous to biological catalysis. *ChemCatChem 2*, 724−761.
(35) Klauss, A., Haumann, M., and Dau, H. (2012) Alternating electron and proton transfer steps in photosynthetic water oxidation. *Proc. Natl. Acad. Sci. U.S.A. 109*, 16035−16040.
(36) McEvoy, J. P., and Brudvig, G. W. (2004) Structure-based mechanism of photosynthetic water oxidation. *Phys. Chem. Chem. Phys. 6*, 4754−4763.
(37) Ishikita, H., and Knapp, E.-W. (2006) Function of redox-active tyrosine in Photosystem II. *Biophys. J. 90*, 3886−3896.
(38) Ferreira, K. N., Iverson, T. M., Maghlaoui, K., Barber, J., and Iwata, S. (2004) Architecture of the photosynthetic oxygen-evolving center. *Science 303*, 1831−1838.
(39) Loll, B., Kern, J., Saenger, W., Zouni, A., and Biesiadka, J. (2005) Towards complete cofactor arrangement in the 3.0 Å resolution structure of Photosystem II. *Nature 438*, 1040−1044.
(40) Guskov, A., Kern, J., Gabdulkhakov, A., Broser, M., Zouni, A., and Saenger, W. (2009) Cyanobacterial Photosystem II at 2.9-Å resolution and the role of quinones, lipids, channels, and chloride. *Nature Struct. Mol. Biol. 16*, 334−342.
(41) Barber, J., Ferreira, K. N., Maghlaoui, K., and Iwata, S. (2004) Structural model of the oxygen-evolving centre of Photosystem II with mechanistic implications. *Phys. Chem. Chem. Phys. 6*, 4737−4742.
(42) De Las Rivas, J., and Barber, J. (2004) Analysis of the structure of the PsbO protein and its implications. *Photosynth. Res. 81*, 329−343.
(43) Bondar, A.-N., and Dau, H. (2012) Exptended protein/water H-bond networks in photosynthetic water oxidation. *Biochim. Biophys. Acta 1817*, 1177−1190.
(44) Linke, K., and Ho, F. M. (2013) Water in Photosystem II: structural, functional, and mechanistic considerations. *Biochim. Biophys. Acta 1837*, 14−32.
(45) Ishikita, H., Saenger, W., Loll, B., Biesiadka, J., and Knapp, E.-W. (2006) Energetics of a possible proton exit pathway for water oxidation in Photosystem II. *Biochemistry 45*, 2063−2071.
(46) Ho, F. M., and Styring, S. (2008) Access channels and methanol binding site to the $CaMn_4$ cluster in Photosystem II based on solvent accessibility simulation, with implications for substrate water access. *Biochim. Biophys. Acta 1777*, 140−153.
(47) Murray, J. W., and Barber, J. (2007) Structural characteristics of channels and pathways in Photosystem II including the identification of an oxygen channel. *J. Struct. Biol. 159*, 228−237.
(48) Gabdulkhakov, A., Guskov, A., Broser, M., Kern, J., Müh, F., Saenger, W., and Zouni, A. (2009) Probing the accessibility of the Mn_4Ca cluster in Photosystem II: channels calculation, noble gas derivatization, and cocrystallization with DMSO. *Structure 17*, 1223−1234.
(49) Vassiliev, S., Comte, P., Mahboob, A., and Bruce, D. (2010) Tracking the flow of water through Photosystem II using molecular dynamics and streamline tracing. *Biochemistry 49*, 1873−1881.
(50) Vassiliev, S., Zaraiskaya, T., and Bruce, D. (2012) Exploring the energetics of water permeation in photosystem II by multiple steered molecular dynamics simulations. *Biochim. Biophys. Acta 1817*, 1671−1678.
(51) Vassiliev, S., Zaraiskaya, T., and Bruce, D. (2013) Molecular dynamics simulations reveal highly permeable oxygen exit channels shared with water uptake channels in photosystem II. *Biochim. Biophys. Acta 1827*, 1148−1155.
(52) Ogata, K., Yuki, T., Hatakeyama, M., Uchida, W., and Nakamura, S. (2013) All-atom molecular dynamics simulation of Photosystem II embedded in thylakoid membranes. *J. Am. Chem. Soc. 135*, 15670−15673.
(53) Frankel, L. K., Sallans, L., Limbach, P. A., and Bricker, T. M. (2012) Identification of oxidized amino acid residues in the vicinity of the Mn_4CaO_5 cluster of Photosystem II: implications for the identification of oxygen channels within the photosystem. *Biochemistry 51*, 6371−6377.
(54) Frankel, L. K., Sallans, L., Bellamy, H., Goettert, J. S., Limbach, P. A., and Bricker, T. M. (2013) Radiolytic mapping of solvent-contact surfaces in Photosystem II of higher plants. *J. Biol. Chem. 288*, 23565−23572.
(55) Ho, F. M. (2008) Uncovering channels in photosystem II by computer modeling: current progress, future prospects, and lessons from analogous systems. *Photosyn. Res. 98*, 503−522.
(56) Ho, F. M. (2012) Substrate and Proton Channels in Photosystem II, in *Molecular Solar Fuels* (Wydrzynski, T. and Hillier, W., Eds.) pp 208−248, Royal Society of Chemistry, Cambridge, UK.
(57) Ho, F. M. (2012) Structural and mechanistic investigations of photosystem II through computational methods. *Biochim. Biophys. Acta 1817*, 106−120.
(58) Hundelt, M., Hays, A.-M. A., Debus, R. J., and Junge, W. (1998) Oxygenic Photosystem II: the mutation D1-D61N in *Synechocystis* sp. PCC 6803 retards S-state transitions without affecting electron transfer from $Y_{Z\ to}\ P_{680}^{+}$. *Biochemistry 37*, 14450−14456.
(59) Clausen, J., Debus, R. J., and Junge, W. (2004) Time-resolved oxygen production by PSII: chasing chemical intermediates. *Biochim. Biophys. Acta 1655*, 184−194.
(60) Service, R. J., Hillier, W., and Debus, R. J. (2010) Evidence from FTIR difference spectroscopy of an extensive network of hydrogen bonds near the oxygen-evolving Mn_4Ca cluster of Photosystem II involving D1-Glu65, D2-Glu312, and D1-Glu329. *Biochemistry 49*, 6655−6669.
(61) Dilbeck, D. L., Hwang, H. J., Zaharieva, I., Gerencser, L., Dau, H., and Burnap, R. L. (2012) The D1-D61N mutation in *Synechocystis* sp. PCC 6803 allows the observation of pH-sensitive intermediates in the formation and release of O_2 from Photosystem II. *Biochemistry 51*, 1079−1091.
(62) Zscherp, C., and Barth, A. (2001) Reaction-induced infrared difference spectroscopy for the study of protein reaction mechanisms. *Biochemistry 40*, 1875−1883.

(63) Barth, A., and Zscherp, C. (2002) What vibrations tell us about proteins. *Q. Rev. Biophys. 35*, 369−430.
(64) Rich, P. R. and Iwaki, M. (2005) Infrared Protein Spectroscopy as a Tool to Study Protonation Reactions Within Proteins, in *Biopysical and Structural Aspects of Bioenergetics* (Wikström, M., Ed.) pp 314−333, Royal Society of Chemistry, Cambridge, U.K.
(65) Barth, A. (2007) Infrared spectroscopy of proteins. *Biochim. Biophys. Acta 1767*, 1073−1101.
(66) Berthomieu, C., and Hienerwadel, R. (2009) Fourier transform infrared (FTIR) spectroscopy. *Photosynth. Res. 101*, 157−170.
(67) Noguchi, T. (2007) Light-induced FTIR difference spectroscopy as a powerful tool toward understanding the molecular mechanism of photosynthetic oxygen evolution. *Photosynth. Res. 91*, 59−69.
(68) Noguchi, T. (2008) Fourier transform infrared analysis of the photosynthetic oxygen-evolving center. *Coord. Chem. Rev. 251*, 336−346.
(69) Chu, H.-A. (2013) Fourier transform infrared difference spectroscopy for studying the molecular mechanism of photosynthetic water oxidation. *Frontiers Plant Sci. 4*, 146−146.
(70) Noguchi, T. (2013) Monitoring the reactions of photosynthetic water oxidation using infrared spectroscopy. *Biomed. Spectrosc. Imaging 2*, 115−128.
(71) Kandori, H. (2000) Role of internal water molecules in bacteriorhodopsin. *Biochim. Biophys. Acta 1460*, 177−191.
(72) Kandori, H., and Shichida, Y. (2000) Direct observation of the bridged water stretching vibrations inside a protein. *J. Am. Chem. Soc. 122*, 11745−11746.
(73) Shibata, M., and Kandori, H. (2005) FTIR studies of internal water molecules in the Schiff base region of bacteriorhodopsin. *Biochemistry 44*, 7406−7413.
(74) Garczarek, F., Brown, L. S., Lanyi, J. K., and Gerwert, K. (2005) Proton binding within a membrane protein by a protonated water cluster. *Proc. Natl. Acad. Sci. U.S.A. 102*, 3633−3638.
(75) Garczarek, F., and Gerwert, K. (2006) Functional waters in intraprotein proton transfer monitored by FTIR difference spectroscopy. *Nature 439*, 109−112.
(76) Freier, E., Wolf, S., and Gerwert, K. (2011) Proton transfer via a transient linear water-molecule chain in a membrane protein. *Proc. Natl. Acad. Sci. U.S.A. 108*, 11435−11439.
(77) Furutani, Y., and Kandori, H. (2014) Hydrogen-bonding changes of internal water molecules upon the actions of microbial rhodopsins studied by FTIR spectroscopy. *Biochim. Biophys. Acta 1837*, 598−605.
(78) Breton, J., and Nabedryk, E. (1998) Proton uptake upon quinone reduction in bacterial reaction centers: IR signature and possible participation of a highly polarizable hydrogen bond network. *Photosynth. Res. 55*, 301−307.
(79) Nabedryk, E., and Breton, J. (2008) Coupling of electron transfer to proton uptake at the QB site of the bacterial reaction center: a perspective from FTIR difference spectroscopy. *Biochim. Biophys. Acta 1777*, 1229−1248.
(80) Iwata, T., Paddock, M. L., Okamura, M. Y., and Kandori, H. (2009) Identification of FTIR bands due to internal water molecules around the quinone binding sites in the reaction center from *Rhodobacter sphaeroides*. *Biochemistry 48*, 1220−1229.
(81) Maréchal, A., and Rich, P. R. (2011) Water molecule reorganization in cytochrome *c* oxidase revealed by FTIR spectroscopy. *Proc. Natl. Acad. Sci. U.S.A. 108*, 8634−8638.
(82) Noguchi, T., and Sugiura, M. (2000) Structure of an active water molecule in the water-oxidizing complex of Photosystem II as studied by FTIR spectroscopy. *Biochemistry 39*, 10943−10949.
(83) Noguchi, T., and Sugiura, M. (2002) FTIR detection of water reactions during the flash-induced S-state cycle of the photosynthetic water-oxidizing complex. *Biochemistry 41*, 15706−15712.
(84) Noguchi, T. (2007) FTIR Detection of water reactions in the oxygen-evolving center of Photosystem II. *Philos. Trans. R. Soc., B 363*, 1189−1195.
(85) Suzuki, H., Sugiura, M., and Noguchi, T. (2008) Monitoring water reactions during the S-state cycle of the photosynthetic water-oxidizing center: detection of the DOD bending vibrations by means of Fourier transform infrared spectroscopy. *Biochemistry 47*, 11024−11030.
(86) Shimada, Y., Suzuki, H., Tsuchiya, T., Tomo, T., Noguchi, T., and Mimuro, M. (2009) Effect of a single-amino acid substitution of the 43 kDa chlorophyll protein on the oxygen-evolving reaction of the Cyanobacterium *Synechocystis* sp. PCC 6803: analysis of the Glu354Gln mutation. *Biochemistry 48*, 6095−6103.
(87) Hou, L.-H., Wu, C.-M., Huang, H.-H., and Chu, H.-A. (2011) Effects of ammonia on the structure of the oxygen-evolving complex in Photosystem II as revealed by light-induced FTIR difference spectroscopy. *Biochemistry 50*, 9248−9254.
(88) Service, R. J., Yano, J., Dilbeck, D. L., Burnap, R. L., Hillier, W., and Debus, R. J. (2013) Participation of glutamate-333 of the D1 polypeptide in the ligation of the Mn_4CaO_5 cluster in Photosystem II. *Biochemistry 52*, 8452−8464.
(89) Noguchi, T., Suzuki, H., Tsuno, M., Sugiura, M., and Kato, C. (2012) Time-resolved infrared detection of the proton and protein dynamics during photosynthetic oxygen evolution. *Biochemistry 51*, 3205−3214.
(90) Polander, B. C., and Barry, B. A. (2013) Detection of an intermediary, protonated water cluster in photosynthetic oxygen evolution. *Proc. Natl. Acad. Sci. U.S.A. 110*, 10634−10639.
(91) Chu, H.-A., Nguyen, A. P., and Debus, R. J. (1994) Site-directed Photosystem II mutants with perturbed oxygen evolving properties: 1. Instability or inefficient assembly of the manganese cluster *in vivo*. *Biochemistry 33*, 6137−6149.
(92) Debus, R. J., Campbell, K. A., Gregor, W., Li, Z.-L., Burnap, R. L., and Britt, R. D. (2001) Does histidine 332 of the D1 polypeptide ligate the manganese cluster in Photosystem II? An electron spin echo envelope modulation study. *Biochemistry 40*, 3690−3699.
(93) Strickler, M. A., Walker, L. M., Hillier, W., Britt, R. D., and Debus, R. J. (2007) No evidence from FTIR difference spectroscopy that aspartate-342 of the D1 polypeptide ligates a Mn ion that undergoes oxidation during the S_0 to S_1, S_1 to S_2, or S_2 to S_3 transitions in Photosystem II. *Biochemistry 46*, 3151−3160.
(94) Strickler, M. A., Walker, L. M., Hillier, W., and Debus, R. J. (2005) Evidence from biosynthetically incorporated strontium and FTIR difference spectroscopy that the C-terminus of the D1 polypeptide of Photosystem II does not ligate calcium. *Biochemistry 44*, 8571−8577.
(95) Tang, X.-S., and Diner, B. A. (1994) Biochemical and spectroscopic characterization of a new oxygen-evolving Photosystem II core complex from the Cyanobacterium *Synechocystis* sp. PCC 6803. *Biochemistry 33*, 4594−4603.
(96) Boussac, A., Rappaport, F., Carrier, P., Verbavatz, J.-M., Gobin, R., Kirilovsky, D., Rutherford, A. W., and Sugiura, M. (2004) Biosynthetic Ca^{2+}/Sr^{2+} exchange in the Photosystem II oxygen-evolving enzyme of *Thermosynechococcus elongatus*. *J. Biol. Chem. 279*, 22809−22819.
(97) Lakshmi, K. V., Reifler, M. J., Chisholm, D. A., Wang, J. Y., Diner, B. A., and Brudvig, G. W. (2002) Correlation of the cytochrome c_{550} content of cyanobacterial Photosystem II with the EPR properties of the oxygen-evolving complex. *Photosynth. Res. 72*, 175−189.
(98) Yamanari, T., Kimura, Y., Mizusawa, N., Ishii, A., and Ono, T.-A. (2004) Mid- to low-frequency Fourier transform infrared spectra of S-state cycle for photosynthetic water oxidation in *Synechocystis* sp. PCC 6803. *Biochemistry 43*, 7479−7490.
(99) Debus, R. J., Strickler, M. A., Walker, L. M., and Hillier, W. (2005) No evidence from FTIR difference spectroscopy that aspartate-170 of the D1 polypeptide ligates a manganese ion that undergoes oxidation during the S_0 to S_1, S_1 to S_2, or S_2 to S_3 transitions in Photosystem II. *Biochemistry 44*, 1367−1374.
(100) Strickler, M. A., Hillier, W., and Debus, R. J. (2006) No evidence from FTIR difference spectroscopy that glutamate-189 of the D1 polypeptide ligates a Mn ion that undergoes oxidation during the S_0 to S_1, S_1 to S_2, or S_2 to S_3 transitions in Photosystem II. *Biochemistry 45*, 8801−8811.

(101) Noguchi, T., and Sugiura, M. (2002) Flash-induced FTIR difference spectra of the water oxidizing complex in moderately hydrated Photosystem II core films: effect of hydration extent on S-state transitions. *Biochemistry 41*, 2322−2330.
(102) Hays, A.-M. A., Vassiliev, I. R., Golbeck, J. H., and Debus, R. J. (1998) Role of D1-His190 in proton-coupled electron transfer reactions in Photosystem II: a chemical complementation study. *Biochemistry 37*, 11352−11365.
(103) Kimura, Y., Mizusawa, N., Ishii, A., Yamanari, T., and Ono, T.-A. (2003) Changes of low-frequency vibrational modes induced by universal ^{15}N- and ^{13}C-isotope labeling in S2/S1 FTIR difference spectrum of oxygen-evolving complex. *Biochemistry 42*, 13170−13177.
(104) Noguchi, T., Sugiura, M., and Inoue, Y. (1999) FTIR Studies on the Amino-Acid Ligands of the Photosynthetic Oxygen-Evolving Mn-Cluster, in *Fourier Transform Spectroscopy: Twelfth International Conference* (Itoh, K., and Tasumi, M., Eds.) pp 459−460, Waseda University Press, Tokyo, Japan.
(105) Noguchi, T., and Sugiura, M. (2003) Analysis of flash-induced FTIR difference spectra of the S-state cycle in the photosynthetic water-oxidizing complex by uniform ^{15}N and ^{13}C isotope labeling. *Biochemistry 42*, 6035−6042.
(106) Service, R. J., Yano, J., McConnell, I., Hwang, H. J., Niks, D., Hille, R., Wydrzynski, T., Burnap, R. L., Hillier, W., and Debus, R. J. (2011) Participation of glutamate-354 of the CP43 polypeptide in the ligation of manganese and the binding of substrate water in Photosystem II. *Biochemistry 50*, 63−81.
(107) Pokhrel, R., Service, R. J., Debus, R. J., and Brudvig, G. W. (2013) Mutation of lysine 317 in the D2 subunit of Photosystem II alters chloride binding and proton transport. *Biochemistry 52*, 4758−4773.
(108) Tommos, C., and Babcock, G. T. (2000) Proton and hydrogen currents in photosynthetic water oxidation. *Biochim. Biophys. Acta 1458*, 199−219.
(109) Wraight, C. A. (2006) Chance and design − proton transfer in water, channels and bioenergetic proteins. *Biochim. Biophys. Acta 1757*, 886−912.
(110) Silverman, D. N., and McKenna, R. (2007) Solvent-mediated proton transfer in catalysis by carbonic anhydrase. *Acc. Chem. Res. 40*, 669−675.
(111) Mikulski, R. L., and Silverman, D. N. (2010) Proton transfer in catalysis and the role of proton shuttles in carbonic anhydrase. *Biochim. Biophys. Acta 1804*, 422−426.
(112) Okamura, M. Y., Paddock, M. L., Graige, M. S., and Feher, G. (2000) Proton and electron transfer in bacterial reaction centers. *Biochim. Biophys. Acta 1458*, 148−163.
(113) Paddock, M. L., Feher, G., and Okamura, M. Y. (2003) Proton transfer pathways and mechanism in bacterial reaction centers. *FEBS Lett. 555*, 45−50.
(114) Wraight, C. A. (2005) Intraprotein Proton Transfer - Concepts and Realities from the Bacterial Photosynthetic Reaction Center, in *Biophysical and Structural Aspects of Bioenergetics* (Wikström, M., Ed.) pp 273−313, RSC Publishing, Cambridge, UK.
(115) Lee, J. L., Reimann, J., Huang, Y., and Ädelroth, P. (2012) Functional proton transfer pathways in the heme-copper oxidase superfamily. *Biochim. Biophys. Acta 1817*, 537−544.
(116) van Ballmoos, C., Ädelroth, P., Gennis, R. B., and Brzezinski, P. (2012) Proton transfer in ba_3 cytochrome *c* oxidase from *Thermus thermophilus*. *Biochim. Biophys. Acta 1817*, 650−657.
(117) Rich, P. R., and Maréchal, A. (2013) Functions of the hydrophilic channels in protonmotive cytochrome *c* oxidase. *J. R. Soc. Interface*, DOI: 10.1098/rsif.2013.0183.
(118) Service, R. J., Hillier, W., and Debus, R. J. (2014) A network of hydrogen bonds near the oxygen-evolving Mn_4CaO_5 cluster of Photosystem II probed with FTIR difference spectroscopy. *Biochemistry 53*, 1001−1017.
(119) Suzuki, H., Yu, J., Kobayashi, T., Nakanishi, H., Nixon, P. J., and Noguchi, T. (2013) Functional roles of D2-Lys317 and the interacting chloride ion in the water oxidation reaction of Photosystem II as revealed by fourier transform infrared analysis. *Biochemistry 52*, 4748−4757.
(120) Noguchi, T., Inoue, Y., and Tang, X.-S. (1999) Structure of a histidine ligand in the photosynthetic oxygen-evolving complex as studied by light-induced fourier transform infrared spectroscopy. *Biochemistry 38*, 10187−10195.
(121) Breton, J., Lavergne, J., Wakeham, M. C., Nabedryk, E., and Jones, M. R. (2007) The unusually strong hydrogen bond between the carbonyl of Q_A and His M219 in the *Rhodobacter sphaeroides* reaction center is not essential for efficient electron transfer from Q_A^- to Q_B. *Biochemistry 46*, 6468−6476.
(122) Saygin, Ö., and Witt, H. T. (1984) On the change of the charges in the four photo-induced oxidation steps of the water-splitting enzyme system S: optical characterization at O_2-evolving complexes isolated from *Synechococcus*. *FEBS Lett. 176*, 83−87.
(123) Saygin, Ö., and Witt, H. T. (1985) Evidence for the electrochromic identification of the change of charges in the four oxidation steps of the photoinduced water cleavage in photosynthesis. *FEBS Lett. 187*, 224−226.
(124) Rappaport, F., Blanchard-Desce, M., and Lavergne, J. (1994) Kinetics of electron transfer and electrochromic change during the redox transitions of the photosynthetic oxygen-evolving complex. *Biochim. Biophys. Acta 1184*, 178−192.
(125) Kretschmann, H., Schlodder, E., and Witt, H. T. (1996) Net charge oscillation and proton release during water oxidation in photosynthesis: an electrochromic band shift study at pH=5.5−7.0. *Biochim. Biophys. Acta 1274*, 1−8.
(126) Mulkidjanian, A., Cherepanov, D., Haumann, M., and Junge, W. (1996) Photosystem II of green plants: topology of core pigments and redox cofactors as inferred from electrochromic difference spectra. *Biochemistry 35*, 3093−3107.
(127) Ahlbrink, R., Haumann, M., Cherepanov, D., Bögershausen, O., Mulkidjanian, A., and Junge, W. (1998) Function of tyrosine-Z in water oxidation by Photosystem II: electrostatical promotor instead of hydrogen abstractor. *Biochemistry 37*, 1131−1142.
(128) Rappaport, F., and Lavergne, J. (1991) Proton release during successive oxidation steps of the photosynthetic water oxidation process: stoichiometries and pH dependence. *Biochemistry 30*, 10004−10012.
(129) Schlodder, E., and Witt, H. T. (1999) Stoichiometry of proton release from the catalytic center in photosynthetic water oxidation - reexamination by a glass electrode study at pH 5.5−7.2. *J. Biol. Chem. 274*, 30387−30392.
(130) Brettel, K., Schlodder, E., and Witt, H. T. (1984) Nanosecond reduction kinetics of photooxidized chlorophyll a_{II} (P-680) in single flashes as a probe for the electron pathway, H^+-release and charge accumulation in the O_2-evolving complex. *Biochim. Biophys. Acta 766*, 403−415.
(131) Meyer, B., Schlodder, E., Dekker, J. P., and Witt, H. T. (1989) O_2 Evolution and Chl a_{II}^+ ($P\text{-}680^+$) nanosecond reduction kinetics in single flashes as a function of pH. *Biochim. Biophys. Acta 974*, 36−43.
(132) Jeans, C., Schilstra, M. J., and Klug, D. R. (2002) The temperature dependence of P_{680}^+ reduction in oxygen-evolving Photosystem II. *Biochemistry 41*, 5015−5023.